Generation and Detection of Higher Harmonics in Rayleigh Waves Using Laser Ultrasound

A Thesis
Presented to
The Academic Faculty

by

Jan Herrmann

In Partial Fulfillment
of the Requirements for the Degree
Master of Science in Engineering Science and Mechanics

School of Civil and Environmental Engineering
Georgia Institute of Technology
December 2005

Generation and Detection of Higher Harmonics in Rayleigh Waves Using Laser Ultrasound

Approved by:

Dr. Laurence Jacobs, Committee Chair
School of Civil and Environmental Engineering
Georgia Institute of Technology

Dr. Jianmin Qu, Committee Chair
George W. Woodruff School of Mechanical Engineering
Georgia Institute of Technology

Dr. Jin-Yeon Kim
George W. Woodruff School of Mechanical Engineering
Georgia Institute of Technology

Date Approved: August 24, 2005

ACKNOWLEDGEMENTS

First of all, i would like to thank my advisor Prof. Laurence J. Jacobs for all his support during my stay in Atlanta. He helped me in desperate situations and motivated me whenever it was necessary. Because of his financial and organizational commitment, i could present the results of this thesis at the Quantitative Nondestructive Evaluation (QNDE) conference in Brunswick, Maine. I also want to thank Dr. Jin-Yeon Kim for all the fruitful discussions and the good coffee we had together. He helped me in an outstanding way to finish the experiments. I thank Prof. Jianmin Qu for his support and for giving me access to the facilities of the School of Mechanical Engineering. Moreover, i want to thank Prof. Thomas E. Michaels and Prof. Jennifer E. Michaels for letting me use their lapping machine and Kritsakorn Luangvilai for showing me how to use the laser interferometer.

Special thanks go to Prof. Lothar Gaul for choosing me as a candidate for the ISAP Program which is financially supported by the DAAD (German Academic Exchange Service). The DAAD is gratefully acknowledged for supporting me with its scholarship. I also want to thank Matthias Maess for his help in organizing the exchange program.

Furthermore i would like to express my deepest gratitude to my family who is supporting me in an extraordinary way. I also want to thank all my friends in Germany and all my new friends in the U.S. Special thanks go to Ben, Helge, Thorsten (Spoon), Eak and Bo for the great working atmosphere in the lab. Last, but not least, i want to thank Ying Shanna Zhou for her love and patience with me.

TABLE OF CONTENTS

LIST OF TABLES

LIST OF FIGURES

LIST OF SYMBOLS OR ABBREVIATIONS

t_i	traction
δ_{ij}	Kronecker delta
b_i	body forces
v	velocity
ρ	density
ϵ_{ij}	strain tensor
σ_{ij}	stress tensor
$\mathbf{u}$	displacement
λ, μ	Lamé constants
ν	Poisson's ratio
ω	angular frequency
$\boldsymbol{\psi}$, φ	displacement potentials
∇	differential operator
A	amplitude
C_{L}	phase velocity of a longitudinal wave
C_{T} or C_{S}	phase velocity of a shear wave
C_{R}	phase velocity of a Rayleigh wave
$\mathbf{d}$	direction of particle motion
E	Young's modulus
G	shear modulus
f	frequency
$\mathbf{p}$	direction of wave propagation
k	wavenumber

λ	wavelength
SNR	signal-to-noise ratio
β	nonlinearity parameter for longitudinal waves
β'	harmonic ratio for Rayleigh waves
A_2^e, A_3^e	Huang coefficients
C_{11}, C_{111}	higher order elastic constants
A_1	amplitude of the fundamental frequency
A_2	amplitude of the second harmonic
b	Burgers vector
h	dipole height
Λ_{dp}	dipole or dislocation density
Ω	conversion factor
ϕ_R	critical angle for Rayleigh wave excitation
t	sample thickness
σ_y	yield stress

SUMMARY

This research studies higher harmonics of Rayleigh surface waves propagating in nickel base superalloys. Rayleigh waves are used because they carry most of the energy and travel along the surface of a specimen where fatigue damage is typically initiated. The energy concentration near the free surface leads to stronger nonlinear effects compared to bulk waves. An ultrasonic piezoelectric transducer together with a plastic wedge is used for the experimental generation of the Rayleigh wave. The detection system consists of a laser heterodyne interferometer. Measurements are performed to detect the fundamental wave as well as the second harmonic. The amplitude ratio is related to the nonlinearity parameter β which is typically used to describe changes in microstructure and investigate fatigue damage.

CHAPTER I

INTRODUCTION

Nonlinear ultrasonics, including the investigation of higher harmonics caused by nonlinear material behavior, has proven to be a useful technique to investigate the condition of structural materials. Monitoring damage accumulation with nonlinear ultrasonics is a new approach in nondestructive evaluation (NDE) which has several advantages when compared to conventional NDE techniques — instead of investigating the existence of individual macro-cracks using the scattered wavefield, nonlinear ultrasonics has the potential to quantify distributed damage on the micro-scale, before the formation of macro-cracks. Rather than waiting for a visible crack, assessment of the early fatigue state is possible. There is enormous potential for the characterization of mechanical and thermal damage such as fatigue, creep, corrosion and over-stress conditions. In addition, nonlinear ultrasonics can help in developing a more fundamental understanding of the contribution of specific changes in microstructure to the accumulation of material damage.

The generation of higher harmonic components in a stress wave propagating through a structural material is a direct result of material nonlinearity (a nonlinear stress-strain relationship) which can be caused by changes in material microstructure. In ultrasonics, these higher harmonics manifest themselves as as a distortion in the transmitted waveform. To quantify the material nonlinearity, harmonic generation measurements have been used to calculate the so-called nonlinearity parameter, β. Previous researchers have shown that changes in β are much more sensitive to material changes than linear ultrasonic properties such as group (or phase) velocity and attenuation.

The reason for the low sensitivity of linear techniques is that the fracture process is initiated at the micro-scale (typically at microscopic imperfections), and this microscopic length scale is much smaller than the typical wavelength of ultrasonic waves.

Several researchers have recently reported dramatic changes in the nonlinearity parameter β in damaged structural materials like high-temperature steel [12], aluminum [8, 18] and titanium [16]. These researchers have tried to associate these changes in β with the formation of dislocations and persistent slip bands, precipitates, vacancies and micro-cracks; theoretical derivations of this association are available in [8] and [7].

So far, most of the research in the area of nonlinear ultrasonics has been concerned with one-dimensional, bulk longitudinal waves. Exceptions are the work of Deng et al. [10], who observe cumulative second harmonic generation of Lamb-wave propagation and the research of Barnard et al. [3] and Blackshire et al. [5] who are considering Rayleigh surface waves. There are three major advantages with using Rayleigh-type surface waves: (i) There is no need for access to both sides of a component for the transmission and detection of Rayleigh waves (one sided access is particularly useful in field applications where two parallel surfaces and two sided access are limited); (ii) Rayleigh waves energy is concentrated near the free surface of a component, which can lead to stronger nonlinear effects compared to bulk waves (this second advantage is additionally critical when considering that fatigue damage is typically initiated on the free surface of a material); and (iii) Rayleigh waves propagate long distances without significant loss of acoustic energy, thus making them ideal candidates for the interrogation of large, complex components.

The primary objective of the current research is to demonstrate the effectiveness

of combining contact wedge generation and non-contact interferometric detection to quantitatively measure the higher harmonics of Rayleigh waves. Once this objective is achieved, a second objective is to investigate the dependence of these higher harmonics on propagation distance (there is a well established analytical relationship between amount of nonlinearity and propagation distance) and then to use the higher harmonics of Rayleigh waves to quantitatively track accumulated micro-damage in a structural material.

Since the second harmonic is directly related to the nonlinearity parameter β, it provides a direct measure of the state of a material's microstructure. This research considers a nickel base superalloy, and tracks these higher harmonics as a function of propagation distance and damage. In addition, this research quantifies the nonlinearity due to the experimental instrumentation, and develops a procedure to reduce this spurious effect.

An outline of the thesis follows. Chapter 2 gives an overview of the fundamentals of wave propagation and wave phenomena. In particular Rayleigh waves and their basic features are described. In chapter 3, an introduction to nonlinear wave propagation is presented. The derivation of the nonlinearity parameter β for longitudinal waves is provided and a link to two-dimensional Rayleigh waves is shown. Chapter 4 presents detailed information about the experimental setup and the associated instrumentation. The wedge method for Rayleigh wave generation is described and the working principle of the laser heterodyne interferometer as a detection system is provided. The experimental results are shown in Chapters 5 and 6 — Chapter 5 investigates the system performance, especially its associated nonlinearities, while Chapter 6 determines material nonlinearity in damaged and undamaged specimens.

CHAPTER II

FUNDAMENTALS OF WAVE PROPAGATION

2.1 Cauchy's Equations of Motion

Consider a collection of material particles occupying a volume V at time t bounded by the surface S (see Figure 2.1). The momentum principle states that the time rate of change of the total momentum of a given set of particles equals the vector sum of all the external forces.

The rate of change of the total momentum of the given mass is $(d/dt)\int \rho v_i dV$, where d/dt is the material derivative of the integral. Then the momentum balance expressed by the postulate is

$$\int_S t_i \mathrm{d}S + \int_V \rho b_i \mathrm{d}V = \frac{d}{dt}\int_V \rho v_i \mathrm{d}V, \tag{2.1}$$

where b are body forces and v denotes the velocity. Now one can substitute the

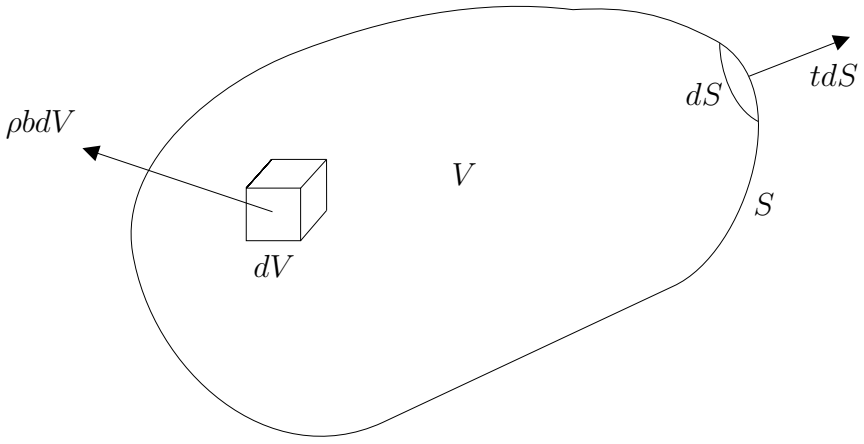

Figure 2.1: Momentum balance

Cauchy formula

$$t_i = \sigma_{ij} n_j \tag{2.2}$$

in the equation above and transform the surface integral by using the divergence theorem to obtain

$$\int_V [\sigma_{ij,j} + \rho b_i - \rho \dot{v}_i] \mathrm{d}V = 0. \tag{2.3}$$

The Reynolds formula was used to transfer the material time derivative inside the integral. Because this equation is valid for an arbitrary volume, one can write

$$\sigma_{ij,j} + \rho b_i = \rho \dot{v}_i \tag{2.4}$$

which are Cauchy's equations of motion. Moreover the moment of momentum principle results in the symmetry of the stress tensor.

Sometimes it is more convenient to write the equations of motion only in terms of the displacements u_i. Applying Hooke's law for a homogeneous, isotropic and linear elastic medium

$$\sigma_{ij} = \lambda \epsilon_{kk} \delta_{ij} + 2\mu \epsilon_{ij}, \tag{2.5}$$

where ϵ_{ij} is the strain tensor related to the displacements u_i by

$$\epsilon_{ij} = \frac{1}{2}(u_{i,j} + u_{j,i}), \tag{2.6}$$

one obtains Navier's equation of motion

$$\mu u_{i,jj} + (\lambda + \mu) u_{j,ji} = \rho \ddot{u}_i \tag{2.7}$$

$$\mu \nabla^2 \mathbf{u} + (\lambda + \mu) \nabla \nabla \cdot \mathbf{u} = \rho \ddot{\mathbf{u}} \tag{2.8}$$

where μ and λ are the Lamé constants. Body forces are neglected in this derivation. (2.8) is a coupled partial differential equation but it can be uncoupled using the Helmholtz decomposition

$$\mathbf{u} = \nabla \varphi + \nabla \times \boldsymbol{\psi}. \tag{2.9}$$

(2.9) represents the three components of displacement u with the four functions φ, ψ_1, ψ_2 and ψ_3. To guarantee the uniqueness of the solution, an additional constraint

$$\nabla \cdot \boldsymbol{\psi} = 0 \tag{2.10}$$

is needed. Substitution of (2.9) into the displacement equations of motion (2.8) leads to two uncoupled wave equations expressed in terms of the displacement potentials φ and $\boldsymbol{\psi}$

$$\nabla^2 \varphi = \frac{1}{c_{\mathrm{L}}^2} \ddot{\varphi}, \qquad \nabla^2 \boldsymbol{\psi} = \frac{1}{c_{\mathrm{T}}^2} \ddot{\boldsymbol{\psi}}, \tag{2.11}$$

whereas c_{L} represents the wave speed of the longitudinal wave (also called dilatational, irrotational, pressure wave or P-wave) and c_{T} the wave speed of the vertically and horizontally polarized shear waves (also called transverse, rotational, distortional wave or S-wave):

$$c_{\mathrm{L}}^2 = \frac{\lambda + 2\mu}{\rho}, \qquad c_{\mathrm{T}}^2 = \frac{\mu}{\rho}. \tag{2.12}$$

(2.11) is the general form of the wave equation, the potentials could also be replaced by the displacements or the strains and the wave equation would still hold.

It is always the case that $c_{\mathrm{L}} > c_{\mathrm{T}}$. Both wave speed equations are expressed in terms of material properties density ρ and the Lamé constants μ and λ. A relationship to material properties Young's modulus E and Poisson's ratio ν is given by

$$\lambda = \frac{E\nu}{(1+\nu)(1-2\nu)}, \tag{2.13}$$

$$\mu = \frac{E}{2(1+\nu)}. \tag{2.14}$$

2.2 Wave Phenomena

Wave phenomena discussed in this section are based on the plane wave assumption, i. e., assuming a wave with constant properties (ϵ, σ, u) on a plane perpendicular to

its direction of propagation $\mathbf{p}$ (propagating vector). The mathematical representation of a plane wave is

$$\mathbf{u} = \mathbf{d} f(\mathbf{x} \cdot \mathbf{p} - ct) \,, \tag{2.15}$$

where $\mathbf{d}$ is the unit vector defining the direction of particle motion (displacement vector), and c is either the longitudinal wave speed c_{L} or the transverse wave speed c_{T}. By substituting (2.15) into (2.8), one obtains

$$(\mu - \rho c^2)\mathbf{d} + (\lambda + \mu)(\mathbf{p} \cdot \mathbf{d})\mathbf{p} = 0 \,. \tag{2.16}$$

Since $\mathbf{p}$ and $\mathbf{d}$ are two different unit vectors, it can be seen that the two possible solutions that form the basis of wave propagation are either $\mathbf{d} = \pm\mathbf{p}$ or $\mathbf{p} \cdot \mathbf{d} = 0$:

1) $\mathbf{d} = \pm\mathbf{p}$ leads to $\mathbf{p} \cdot \mathbf{d} = \pm 1$. Inspection of (2.16) yields $c = c_{\mathrm{L}}$ as defined in (2.12). Since $\mathbf{d}$ and $\mathbf{p}$ are linearly dependent, this represents a particle movement in the direction of propagation – a longitudinal or P-wave.

2) $\mathbf{p} \cdot \mathbf{d} = 0$ leads with (2.12) and (2.16) to $c = c_{\mathrm{T}}$. Hence, the direction of motion is normal to the direction of propagation, and the wave is called a transverse wave. If a two-dimensional plane of propagation is considered (for example, the (x_1, x_2)-plane), a wave with an in-plane displacement (in the (x_1, x_2)-plane) is called an SV-wave (vertically polarized), while a wave with out-of-plane displacement (in the x_3-direction) is called an SH-wave (horizontally polarized).

In a homogeneous, isotropic material, transverse and longitudinal wave speeds are independent of frequency, therefore they are nondispersive.

2.2.1 Reflections of P and SV-Waves

The wave types derived so far propagate independently in an infinite media. As soon as a finite media in the direction of propagation is considered, reflections and coupling will occur. An incident P-wave, which is reflected at a stress free boundary

($\sigma_{22} = 0$ and $\sigma_{21} = 0$) normally causes both a reflected P- and SV-wave. Similarly, an incident SV-wave generally causes both reflected SV- and P-waves. Figure 2.2 shows the reflections of an incident P- and SV-wave.

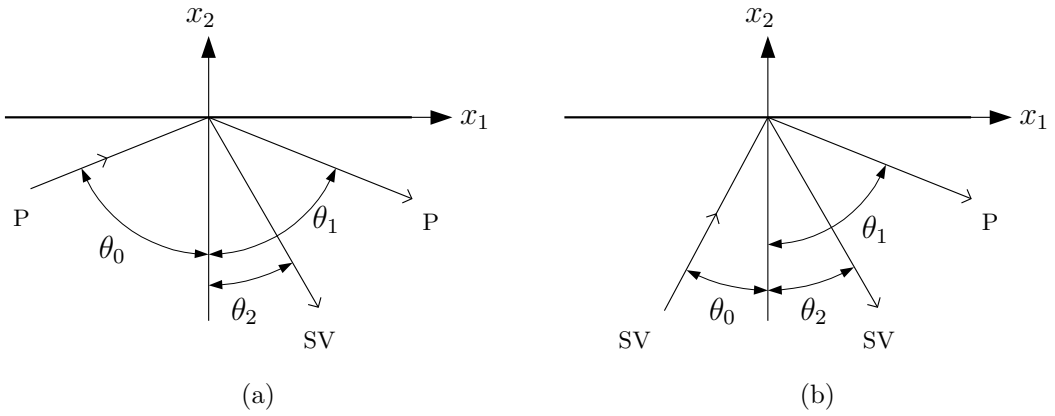

Figure 2.2: Wave reflections. (a) Reflection of a P-wave. (b) Reflection of a SV-wave.

The effect of a single incident wave-type producing two different waves (after reflection from a boundary) is called mode conversion. The displacement field of a harmonic wave in the x_1, x_2 plane (propagating in infinite media, plane-strain case) can be expressed as

$$\mathbf{u}^{(n)} = A_n \mathbf{d}^{(n)} \exp\left[\imath k_n (x_1 p_1^{(n)} + x_2 p_2^{(n)} - c_n t)\right] , \tag{2.17}$$

whereas n denotes the wave (longitudinal or transverse), $k_n = \frac{\omega}{c_n}$ is called the wavenumber of the wave n and the respective wave speeds are c_n. Using these definitions, and noting that the angular frequency ω is equal for the incident and reflected waves, it is possible to determine the relationship between the angle of the incident and the angles of the reflected waves (see Table 2.1). To obtain non-trivial amplitudes A_n, the angles of incident and reflected waves, θ_0, θ_1 and θ_2 as defined in Figure 2.2, must satisfy Snell's law:

$$k_0 \sin\theta_0 = k_1 \sin\theta_1 = k_2 \sin\theta_2 . \tag{2.18}$$

Table 2.1: Angle relations for reflection on a stress-free surface

incident θ_0	reflected P θ_1	reflected SV θ_2
P	$\theta_1 = \theta_0$	$\sin\theta_2 = (c_\mathrm{T}/c_\mathrm{L})\sin\theta_0$
SV	$\sin\theta_1 = (c_\mathrm{L}/c_\mathrm{T})\sin\theta_0$	$\theta_2 = \theta_0$

Exceptions of mode conversion are the normal incidence with $\theta_0 = 0$ — in this case, the waves are reflected as themselves, and if the angle θ_0 is greater than a critical angle

$$\theta_\mathrm{critical} = \arcsin\frac{c_\mathrm{T}}{c_\mathrm{L}}\,, \tag{2.19}$$

then only a SV-wave is reflected. The P-wave portion of the reflected signal degenerates into a Rayleigh surface wave, details about this specific two-dimensional harmonic wave can be found in Section 2.3.

2.3 Rayleigh Waves

Rayleigh waves travel along the free surface of an elastic half space and decay exponentially with depth. On the free boundary these waves cancel the stresses which they produce. Viktorov [27] and Achenbach [1] provide details about the derivations and properties of Rayleigh waves. Moreover Viktorov [27] and Rose [22] describe applications of Rayleigh wave propagation in ultrasonic nondestructive evaluation. In addition excitation methods are explained and compared.

The well-known equation for the phase velocity of Rayleigh waves can be derived starting with the potentials

$$\varphi = Ae^{-kqz}e^{ik(x-ct)} \tag{2.20}$$

$$\phi = Be^{-ksz}e^{ik(x-ct)}, \tag{2.21}$$

where $q = \sqrt{1-(\frac{c}{c_L})^2}$, $s = \sqrt{1-(\frac{c}{c_T})^2}$, $c = \frac{\omega}{k}$ and A, B are arbitrary constants. Using the wave equations (2.11) and applying stress-free boundary conditions lead to

the following characteristic equation

$$\left(2-\frac{C_R^2}{C_S^2}\right)^2-4\sqrt{\left(1-\frac{C_R^2}{C_L^2}\right)\left(1-\frac{C_R^2}{C_S^2}\right)}=0, \tag{2.22}$$

which is the Rayleigh equation showing that the phase velocity of Rayleigh waves does not depend on the wave number, therefore Rayleigh waves are nondispersive. An approximate solution can be obtained as

$$C_R \approx C_S \frac{0.87+1.12\nu}{1+\nu} \tag{2.23}$$

where ν is the Poisson's ratio.

In general the Rayleigh wave speed is less than the phase velocity of the longitudinal or the shear wave. Essentially the Rayleigh wave is a combination of body waves. The particle motion of a propagating Rayleigh wave is elliptical in nature because the displacements along the x and z axis are phase-shifted by $\pi/2$ (see Figure 2.3). The vertical displacement is typically 1.5 times greater than the horizontal component at the surface and the elliptical motion is counter clockwise for a wave traveling along the positive x-direction (a water wave would rotate clockwise). At a depth of around 0.2 times the wavelength, the direction of particle rotation changes.

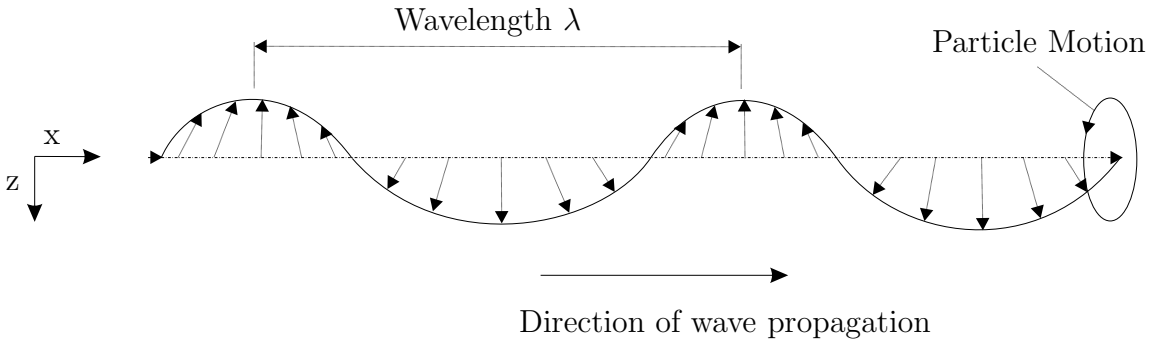

Figure 2.3: Particle motion during propagation of a Rayleigh surface wave

Achenbach [1] also provides numerical details about variations of the displacements with depth. He plots the relative displacement over the ratio of the distance from the free surface and the wavelength and he concludes that the relative displacements

almost vanishes for a distance of more than 1.5 times the wavelength. These results are important for the sample thickness used in the present research.

Another feature of Rayleigh waves is the energy concentration near the free surface. Therefore surface cracks and damage disturbing the traveling wave can be detected. Especially ultrasonic techniques are able to use Rayleigh wave propagation as a means of nondestructive evaluation. Another field of application is seismology where the Rayleigh wave is used to explain high damage of a wave which propagates far distances and still carries most of the energy.

Because the Rayleigh wave follows the surface around, curves can also be used to inspect areas that other waves might have difficulty reaching.

If one considers an interface between two materials instead of an elastic half space, similar derivations lead to the so-called Stonely wave propagating along interfaces.

A thin layer on top of a half space with different elastic properties leads to Love waves. Considering a half-space made of ideal fluid, a Rayleigh-type surface wave propagation is not possible.

CHAPTER III

NONLINEAR WAVE PROPAGATION

Higher harmonics are related to the so called nonlinearity parameter, β. This chapter gives a theoretical background in one dimensional nonlinear wave propagation and the derivation of this nonlinearity parameter. Contribution from lattice elasticity and dislocation dipoles are considered. Moreover the relation to the experimental determination of the second harmonic is shown. A difference between wave propagation in linear and nonlinear medium can be found in Figure 3.1.

Section 3.2 provides a link to nonlinear wave propagation in two-dimensional Rayleigh waves.

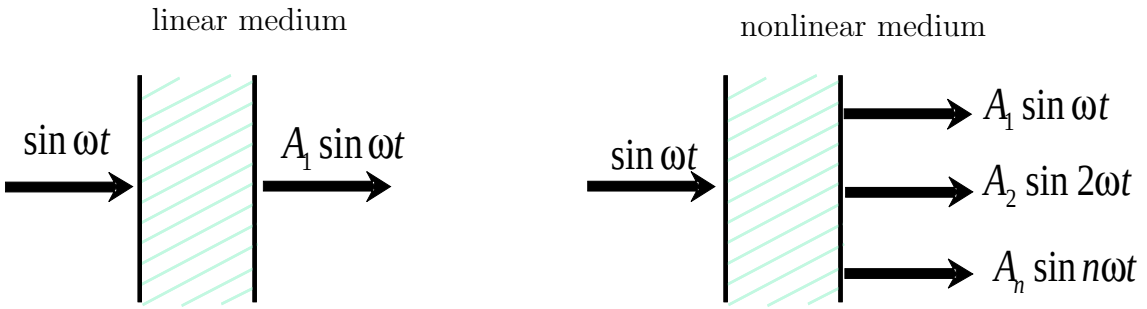

Figure 3.1: Linear and nonlinear wave propagation in solids

3.1 Nonlinearity Parameter β

According to [2], the fundamental wave will distort as it propagates, therefore the second and higher harmonics will be generated. Particularly the lattice anharmonicity and dislocation structures contribute to the nonlinearity parameter. A detailed derivation of β can be found in [7], this section summarizes the main steps and gives an introduction in nonlinear wave propagation.

A longitudinal stress perturbation σ associated with a propagating ultrasonic wave produces a longitudinal strain

$$\epsilon = \epsilon_e + \epsilon_{pl} \tag{3.1}$$

in the material where ϵ_{pl} is the plastic strain component associated with the motion of dislocation in the dipole configuration.

The relation between the stress perturbation and elastic strain can be written in the nonlinear form of Hooke's law (quadratic nonlinear approach)

$$\sigma = A_2^e \epsilon_e + \frac{1}{2} A_3^e \epsilon_e^2 + ... \tag{3.2}$$

or

$$\epsilon_e = \frac{1}{A_2^e}\sigma - \frac{1}{2}\frac{A_3^e}{(A_2^e)^3}\sigma^2 + ... \tag{3.3}$$

where A_2^e and A_3^e are the Huang coefficients.

According to [7], the relation between the stress perturbation and the plastic strain ϵ_{pl} can be obtained from a consideration of dipolar forces. For edge dislocation pairs with opposite polarity, one can write

$$F_x = -\frac{Gb^2}{2\pi(1-\nu)}\frac{x(x^2-y^2)}{(x^2+y^2)^2} \tag{3.4}$$

where b is the Burgers vector, ν is Poisson's ratio, G is the shear modulus and x, y are the Cartesian coordinates of one dislocation in the pair relative to the other. At equilibrium, y=h, where h is the dipole height and the total shear force per unit length on the dipole is

$$F_x + bR\sigma = 0 \tag{3.5}$$

where R is the Schmid factor along slip planes.

Also the relation between ϵ_{pl} and the relative dislocation displacement $\xi = x - h$ is

given by

$$\epsilon_{pl} = \Omega \Lambda_{dp} b \xi \tag{3.6}$$

where Ω is a conversion factor and Λ_{dp} is the dipole density.

Using these relationships among $F_x, \sigma, \epsilon_{pl}, \xi$ and an expansion of (3.4) in a power series in x with respect to h leads to the following equation

$$\sigma = A_2^{dp} \epsilon_{pl} + \frac{1}{2} A_3^{dp} \epsilon_{pl}^2 + ... \tag{3.7}$$

where $A_2^{dp} = -\frac{G}{4\pi\Omega R \Lambda_{dp} h^2 (1-\nu)}$ and $A_3^{dp} = \frac{G}{4\pi\Omega^2 R \Lambda_{dp}^2 h^3 (1-\nu) b}$. The inverse relation is

$$\epsilon_{pl} = \frac{1}{A_2^{dp}} \sigma - \frac{1}{2} \frac{A_3^{dp}}{(A_2^{dp})^3} \sigma^2 + ... \tag{3.8}$$

(3.2) and (3.8) in (3.1) results in

$$\epsilon = \left(\frac{1}{A_2^e} + \frac{1}{A_2^{dp}} \right) \sigma - \frac{1}{2} \left(\frac{A_3^e}{(A_2^e)^3} + \frac{A_3^{dp}}{(A_2^{dp})^3} \right) \sigma^2 + ... \tag{3.9}$$

or the inverse relation

$$\sigma = A_2^e \left[\epsilon - \frac{1}{2} \left(\frac{A_3^e}{A_2^e} + \frac{A_3^{dp} (A_2^e)^2}{(A_2^{dp})^3} \right) \epsilon^2 + ... \right]. \tag{3.10}$$

The wave equation with respect to the Lagrangian coordinate X is given as

$$\rho \frac{\partial^2 \epsilon}{\partial t^2} = \frac{\partial^2 \sigma}{\partial X^2}. \tag{3.11}$$

(3.10) in (3.11) gives

$$\frac{\partial^2 \epsilon}{\partial t^2} - c^2 \frac{\partial^2 \epsilon}{\partial X^2} = -c^2 \beta \left[\epsilon \frac{\partial^2 \epsilon}{\partial X^2} + \left(\frac{\partial \epsilon}{\partial X} \right)^2 \right] \tag{3.12}$$

where $c = (A_2^e/\rho)^{1/2}$ and $\beta = \beta_e + \beta_{dp}$ with $\beta_e = -\frac{A_3^e}{A_2^e}$ and $\beta_{dp} = \frac{16\pi\Omega R^2 \Lambda_{dp} h^3 (1-\nu)^2 (A_2^e)^2}{G^2 b}$.

In the literature, the Huang coefficients are often written in terms of higher elastic constants, that is $A_1^e = C_1$ where C_1 is equal to the initial stress. Moreover, $A_2^e = C_1 + C_{11}$ and $A_3^e = 3C_{11} + C_{111}$. Assuming zero initial stress, the portion of β

describing the nonlinearity contribution from lattice elasticity can be expressed as $\beta_e = -\left(3 + \frac{C_{111}}{C_{11}}\right)$.

Assuming a purely sinusoidal input wave of the form $\epsilon_0 sin(\omega t - kX)$, a solution to (3.12) is

$$\epsilon = \epsilon_0 sin(\omega t - kX) - \frac{1}{4}\beta k \epsilon_0^2 X sin[2(\omega t - kX)]. \tag{3.13}$$

Therefore β can be described by the amplitudes A_1 and A_2 of the fundamental frequency and the second harmonic respectively as

$$\beta = \frac{4k}{X}\frac{A_2}{A_1^2} \tag{3.14}$$

which permits the experimental determination of the nonlinearity parameter.

Similar expressions can be obtained for displacements instead of strains.

Starting with Newton's law, one can write

$$\rho \frac{\partial^2 u}{\partial t^2} = \frac{\partial^2 \sigma}{\partial X^2}. \tag{3.15}$$

(3.10) in (3.15) results in the displacement based nonlinear wave equation

$$\frac{\partial^2 u}{\partial t^2} = c^2 \left[1 - \beta \frac{\partial u}{\partial X}\right] \frac{\partial^2 u}{\partial X^2}. \tag{3.16}$$

Assuming an input wave of the form $u_0 cos(kX - \omega t)$, a solution to equation (3.16) is

$$u = \frac{1}{8}\beta k^2 u_0^2 X + u_0 cos(kX - \omega t) - \frac{1}{8}\beta k^2 u_0^2 X cos[2(kX - \omega t] + ... \tag{3.17}$$

Again, β can be expressed by the amplitudes A_1 and A_2 of the fundamental frequency and the second harmonic respectively which leads to the following expression for β:

$$\beta = 8\frac{A_2}{A_1^2}\frac{c^2}{\omega^2 X} \tag{3.18}$$

or

$$\beta = \left(\frac{A_2}{A_1^2}\right)\frac{2c^2}{X f^2 \pi^2}. \tag{3.19}$$

The nonlinearity parameter β depends on the amplitudes of the fundamental wave as well as the second harmonic, the wave speed, the propagation distance and frequency. If the amplitude of the second harmonic is determined experimentally using a certain frequency and propagation distance, β can be determined.

3.2 Nonlinear Wave Propagation in Rayleigh Waves

The derivation of β mentioned above is only valid for longitudinal waves. This research deals with two-dimensional Rayleigh waves which makes the derivation of the nonlinearity parameter considerably more difficult, although it is obvious that the nonlinearity should depend on the amplitude ratio $\frac{A_2}{A_1^2}$. A modeling approach for nonlinear Rayleigh wave propagation can be found in [26], [21] or [14].

Generally speaking, Rayleigh waves are a superposition of bulk waves. Especially longitudinal waves are sensitive with respect to the generation of higher harmonics whereas shear waves are seen as a wave-type without significant potential for higher harmonic generation in ultrasonic waves. Following this idea, Rayleigh waves should have a similar behavior than longitudinal waves with respect to nonlinear wave propagation.

Measurements of higher harmonics in propagating Rayleigh waves are therefore the critical step in determining nonlinearity in a certain material. The harmonic ratio $\frac{A_2}{A_1^2}$ is used to quantify nonlinear material behavior and is therefore needed to compare specimens with different damage and fatigue states. In the following, the harmonic ratio A_2/A_1^2 is called β'. Because material damage is particularly initiated at the surface, a Rayleigh wave propagating along a damaged specimen is expected to exhibit more nonlinearity compared to the undamaged sample.

Whereas the dimensionless nonlinearity parameter β stays constant for different propagation distances, the amplitude of the second harmonic changes linearly with the propagation distance as required for a quadratic nonlinearity. Because of this information, two different sets of measurements can be conducted:

1.) An increase in propagation distance should result in higher amplitudes of the second harmonic (and note that the dimensionless nonlinearity parameter should stay constant using the same specimen).

2.) The harmonic ratio or β' should increase when the material is more and more damaged or fatigued.

Because the amplitude of higher harmonics are considerably smaller than the one of the fundamental frequency, the major task is to come up with an experimental setup which is sensitive enough to detect higher harmonics. A high signal-to-noise-ratio (SNR) is needed, moreover the experimental setup (e.g. instrumentation) has to be as linear as possible because only the material nonlinearities are of interest and not the contribution of the instrumentation which can create spurious nonlinearities.

With a knowledge of the physics of nonlinear wave propagation, and being aware of the fact that instrumentation has a high influence on nonlinear ultrasonic measurements, one can start creating a reliable and convenient experimental setup.

CHAPTER IV

EXPERIMENTAL PROCEDURE

The experimental procedure is described in the following sections. Two different experimental setups are shown and explained in Section 4.1 and 4.2. Section 4.3 illustrates the different steps required to generate a Rayleigh wave. The detection system is explained in Section 4.4. Finally, details about the specimens and the material are provided.

4.1 Experimental Setup #1

The general experimental setup is illustrated in Figure 4.1. A Wavetek function generator is used to generate a toneburst signal which is amplified with a 50 dB high voltage amplifier (ENI Model 240L RF). The input voltage for the amplifier is limited to 1 V, that's the reason why the experiments with setup #1 are performed with an input voltage of not more than 900 mV. An ultrasonic transducer with a center frequency close to 5 MHz together with a plastic wedge excites the Rayleigh wave propagating along the surface of the specimen. A laser heterodyne interferometer is used as a point-like detection system. Details about the experimental systems are given in the following sections.

Figure 4.2 shows the incident wave excited with the piezoelectric transducer as well as the fundamental wave with the amplitude A_1 and the second harmonic with the amplitude A_2 detected with the laser interferometer system. The frequency of the second harmonic is two times higher than the one of the fundamental.

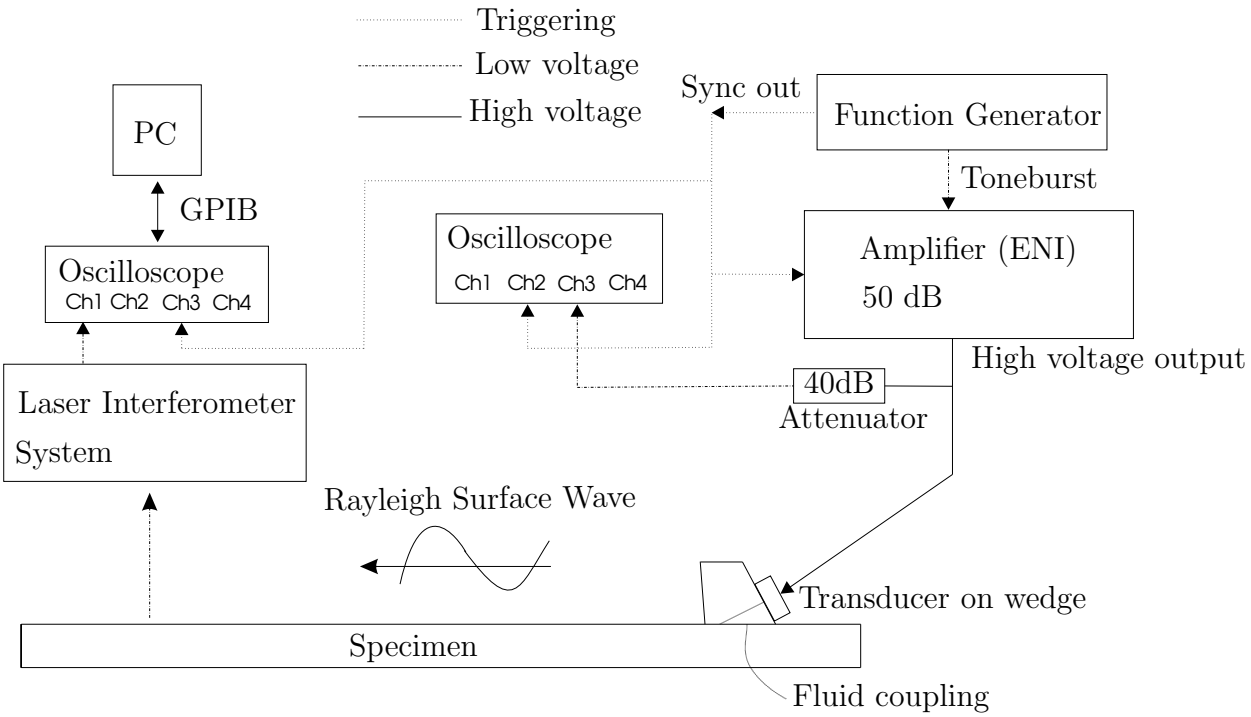

Figure 4.1: Experimental setup #1

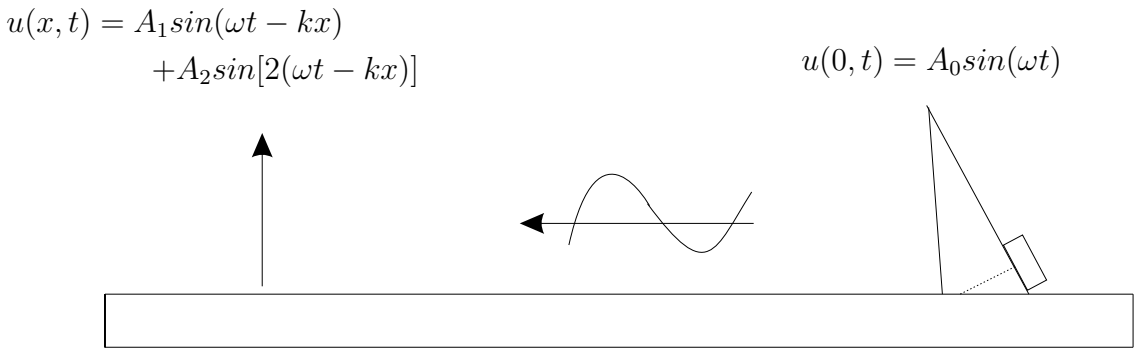

Figure 4.2: Fundamental wave and second harmonic

4.1.1 Transducer

The experiments are conducted with an Ultran KC50-5-X PZT (lead zirconate titanate) ultrasonic transducer with a nominal frequency of 5 MHz. According to the data sheet provided by the Ultran Group, the bandwidth at -6 dB is 6.3 MHz and the bandwidth center frequency is 3.7 MHz with a peak frequency of 4.225 MHz. Because this transducer is broadband in nature, one can use this transducer for a driving frequency of 5 MHz.

To check the data, a simple experiment is performed to see the efficiency of this transducer. A second receiving transducer (Ultran KC50-5) is held firmly against the transmitting transducer and a face-to-face measurement is conducted. The frequency is changed and the change in amplitude is investigated, the amplitude is normalized to get a dimensionless magnitude. Figure 4.3 shows the efficiency plot. One can see that the magnitude decreases considerably after the maximum peak which is not surprising because the receiving transducer has also a resonance frequency below 5 MHz. Nevertheless measurements at 5 MHz can still be performed because of the broadband nature of the transmitting PZT-transducer. Although the efficiency plot shows that the properties of the transducer at 5 MHz are not quite sufficient, one can see at other experiments that this transducer has still a better performance and reliability than other commercial transducers.

Section 5.5.5 deals with nonlinear behavior of transducers and provides a comparison between two different PZT-transducers.

4.1.2 Function Generator

A Wavetek function generator provides toneburst signals at the desired frequency. Moreover the number of cycles and the signal type can be adjusted. Only sinusoidal signals are generated in this research. Moreover the input voltage for the amplifier can be changed with this function generator. Most of the measurements using setup

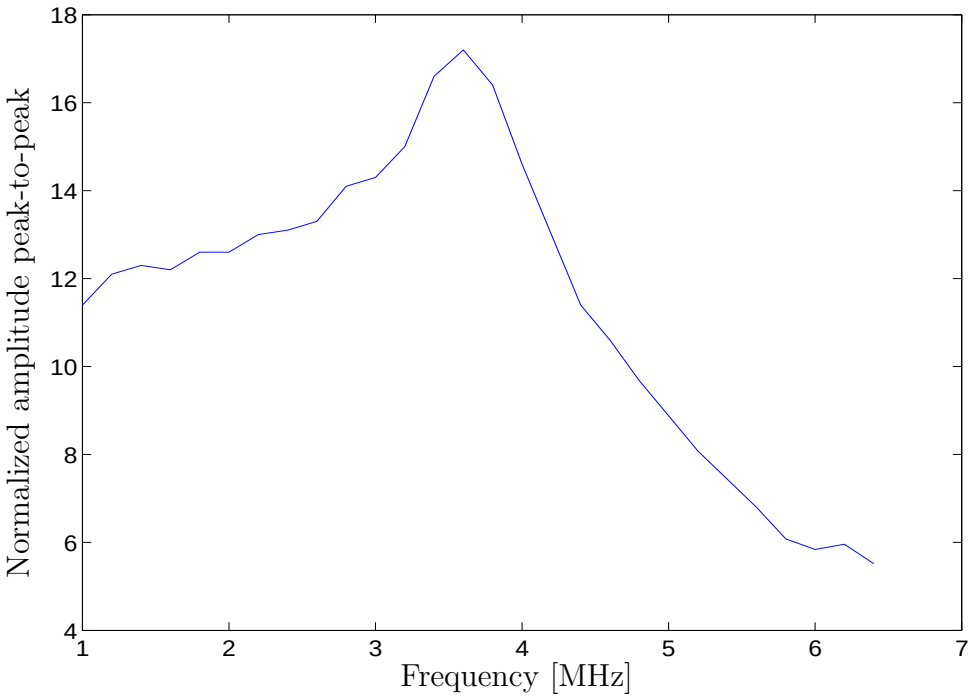

Figure 4.3: Efficiency plot of the transducer

#1 are conducted with 800 mV input.

4.1.3 Amplifier

The amplification factor of the high voltage amplifier (ENI) is 50 dB. Such a conventional power amplifier introduces inherent nonlinearities to the electrical signal, especially odd order harmonics are generated. This is a limiting factor, details about the nonlinearity of the electrical equipment are described in chapter 5.5.4.

With the function generator described above, one can use up to 1 V as an input for the amplifier, therefore up to 316 V can be generated which is the limit for the present 50 dB amplification.

4.2 Experimental Setup #2

This section describes an improved experimental setup. The 50 dB amplifier is replaced by a Ritec high power amplifier (RAM-10000, Ritec Advanced Measurement

System) which was particularly designed for nonlinear acoustic measurements. Several advantages can be pointed out using this gated high power amplifier: The voltage and amplification factor is much higher in comparison to conventional commercial amplifiers (theoretically the output voltage can go up to 1000 V). High voltage is required to detect higher harmonics with relatively small amplitudes which is the case for surface wave propagation in combination with laser detection. The higher the input signal, the easier higher harmonics can be detected. Moreover this amplifier generates a negligible second harmonic and the odd order harmonics are barely affected, therefore it is an ideal means to create high voltage for nonlinear acoustic measurements. Figure 4.4 provides a detailed plot of the experimental setup #2. The Ritec

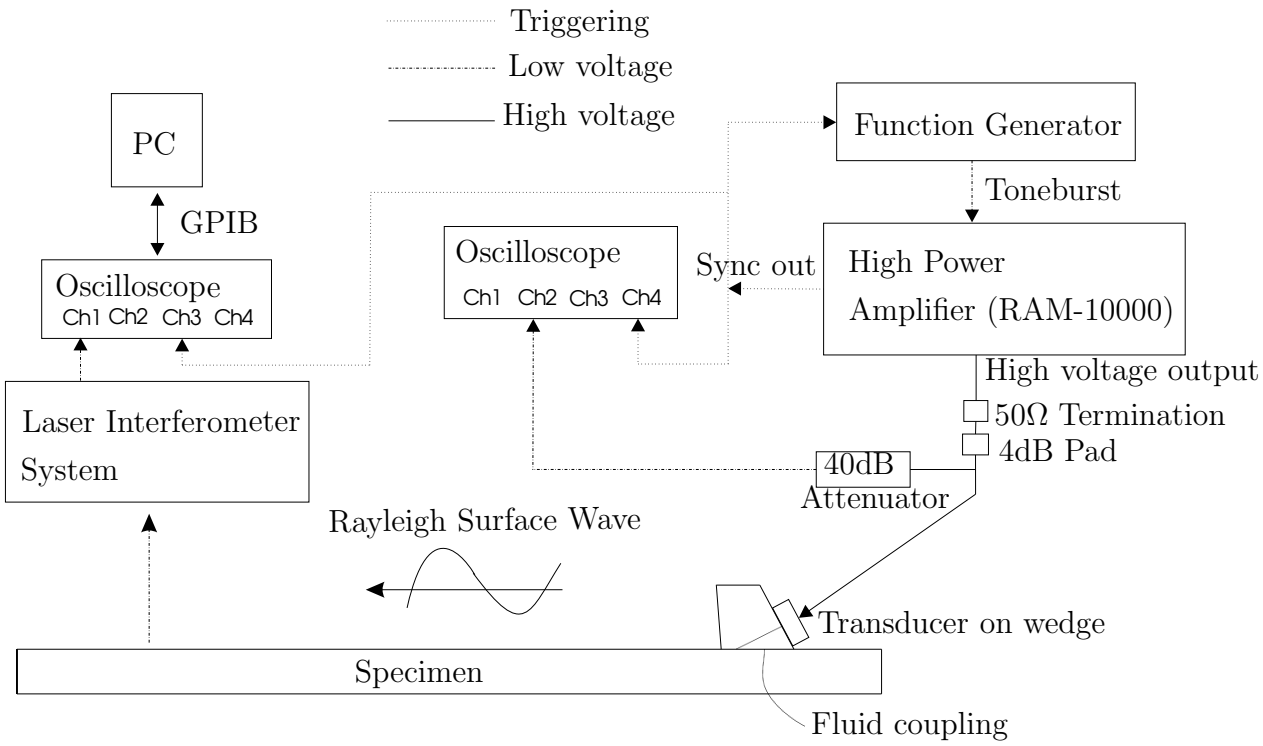

Figure 4.4: Experimental setup #2

amplifier is used as triggering source (sync out), an 80 MHz Agilent 33250A function/arbitrary waveform generator generates the toneburst signal. The input voltage for the Ritec high power amplifier is varied from 1 to 1.13 V, then the signal is amplified and the ultrasonic transducer is driven with 5 MHz. To match the impedance

between the high voltage output of the amplifier and the transducer and to suppress the excessive transient content in the generated toneburst, a 50Ω termination and a 4dB pad are used. The transducer and the detection system are the same as for the conventional setup #1.

4.3 Generation of Rayleigh Surface Waves

The excitation of a Rayleigh surface wave is described in the following. Especially the design and the efficiency of a surface wave generation is pointed out.

4.3.1 Wedge Method

There are several techniques available for the excitation of ultrasonic Rayleigh waves. According to Rose [22], a normal beam transducer excitation can be used for generating surface waves. He also proposed a periodic array or comb transducer and a mediator technique. The most common technique, the wedge method, will be presented in this chapter (see Figure 4.5).

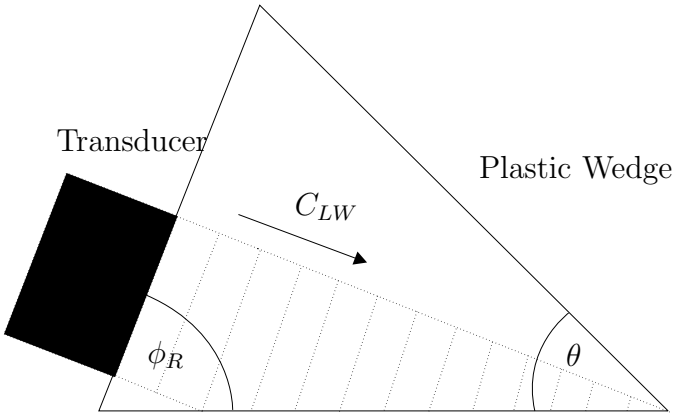

Figure 4.5: Wedge technique

This method is based on a plastic wedge which is coupled to the surface of the solid or specimen. For an appropriate acoustic coupling, oil or cement glues are available. Details about couplants can be found in Section 5.3.2. A piezoelectric transducer is bonded on the sloping surface of the wedge, so that a longitudinal wave can propagate

through the wedge material. This longitudinal wave hits the boundary of the solid and wedge under a certain angle. To generate a surface wave, this angle has to satisfy the Rayleigh Wave excitation condition, which is based on Snell's law (Figure 4.6)

$$sin\phi_2 C_1 = sin\phi_1 C_2 \tag{4.1}$$

where C_1 and C_2 are wave velocities and ϕ_1 and ϕ_2 the incident and refraction angles.

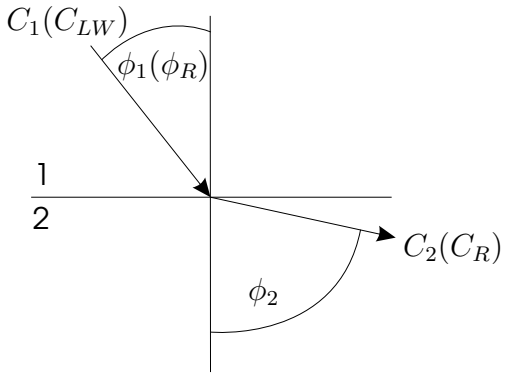

Figure 4.6: Snell's law for angle beam analysis

For the present wedge method, C_1 is the longitudinal wave velocity C_{LW} of the wedge material and C_2 is the Rayleigh wave speed C_R of the specimen. In the case of a longitudinal incident wave, $\phi_2 = 90°$, or $sin\phi_2 = 1$, so that the critical angle ϕ_R for a Rayleigh wave excitation can be computed as

$$sin\phi_R = \frac{C_{LW}}{C_R}. \tag{4.2}$$

C_{LW} must be smaller than C_R, that's the reason why the wedge material is made of plastic like plexiglas where the wave speed is low.

Generally not only a Rayleigh wave will be generated because the transducer is not able to excite a perfectly plane wave. The shape of the beam is rather a Gaussian distribution, therefore the transducer beam does not remain in a cylinder. Instead the beam spreads out as it propagates through the material so that not the whole beam hits the surface at the critical angle. Because of this there will also be some bulk waves generated in the specimen, although the Rayleigh surface wave carries

most of the energy.

The effect described above is called beam divergence or ultrasonic diffraction. In general, the maximum sound pressure is always found along the centerline of the transducer, therefore it is usually called the acoustic axis. The beam strength diminishes as it spreads outwards.

To decrease these effects, it is useful to design the wedge in a way that the propagation distance of the longitudinal wave through the wedge material is as short as possible.

Moreover, the wedge design can be improved in increasing the angle θ in Figure 4.5 to slightly over 90°, so that the reflected waves can propagate to the upper parts of the wedge without interfering the incident longitudinal waves which are used for the conversion into Rayleigh waves.

According to [27], the most efficient excitation can be realized when the leading edge of the piezoelectric transducer coincides with the projection of the wedge to the sloping surface (Figure 4.5), but this is only true if the transducer is able to generate a plane wave. Because of the beam divergence mentioned above, it is more efficient if not the leading edge of the transducer, but the acoustic axis coincides with the projection of the wedge to the sloping surface. Then a clean Rayleigh wave can be excited with the starting point at the leading edge of the wedge.

Ruiz et al. [23] found out that there is a dispersion effect in Rayleigh waves even in nondispersive media on the order of 0.1 percent, particularly because of beam diffraction, but for higher frequencies and a high input voltage these effects are negligible (no diffraction correction is needed) and the propagating Rayleigh wave approaches a true plane wave.

The wedge method is suitable for an application where the Rayleigh wave propagates

only in one direction (like in the present research), especially then it is a highly efficient excitation method because the energy only goes in this particular direction of wave propagation.
To calculate the Rayleigh wave speed of the specimen, one has to determine both the longitudinal and shear wave velocity. According to Achenbach [1], C_R can then be computed numerically from (2.22).

An alternative way to excite the surface wave would be a laser source instead of a plastic wedge - transducer combination. Of course, geometrical effects could be investigated readily, but a laser source is basically a broadband pulse and waves would propagate in all directions. Only if the geometry of the specimen is very simple, a laser source will give conclusive results about geometrical effects, otherwise it would make the observation of wave propagation considerably more difficult. The other disadvantage of the laser source is that the whole frequency bandwidth is involved in the measurements. In this research a particular input frequency is needed to detect higher harmonics, therefore a broadband source is not effective.

4.3.2 Wedge Material and Design

Before the longitudinal wave propagating through the wedge material converts into a Rayleigh wave on the surface of the specimen, several energy losses and disturbances must be considered. First of all the propagation distance through the wedge is a limiting factor. As mentioned above, not the whole beam coming from the transducer contributes to the Rayleigh wave. If the distance between the transducer surface and the specimen is too long, more and more body waves will propagate in the specimen, consequently the Rayleigh wave will carry less energy.
Moreover, the plastic material of the wedge has a relatively high attenuation. That

is, next to the propagation distance, the wedge material itself is important for the efficiency of the Rayleigh wave generation. The less attenuation in the wedge material, the more energy will go into the Rayleigh wave. According to Ginzel [11], polystyrene has the lowest attenuation (attenuation coefficient of 0.2 dB/mm at 5 MHz), followed by plexiglas (attenuation coefficient of 0.6 dB/mm at 5 MHz). Because of this difference in the attenuation properties and the importance of the wedge material for the Rayleigh wave generation, both the attenuation coefficient of polystyrene and plexiglas are determined. The experimental results are shown in this section.

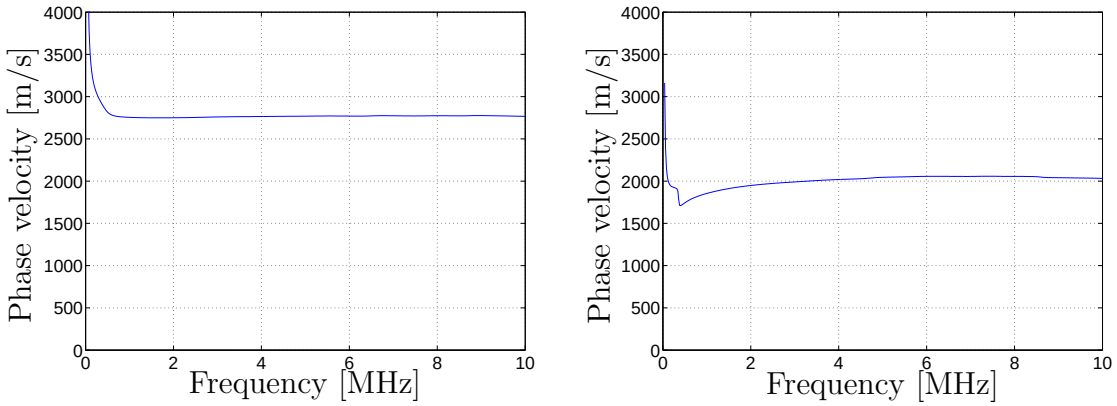

(a) Phase velocity in plexiglas

(b) Phase velocity in polystyrene

Figure 4.7: Phase velocities in polystyrene and plexiglas

To determine the attenuation coefficient, the longitudinal wave velocity of the wedge material has to be known. Because the plastic material is dispersive, the longitudinal wave speed is frequency dependent. According to Sachse and Pao [24], the phase velocity of waves in dispersive media can be calculated based on the phase spectral analysis of a broadband pulse. In this technique, the phase function of a Fourier-analyzed pulse is evaluated. The advantage of this technique is that the phase velocity is directly obtainable from the experimental data.

The results for polystyrene and plexiglas are shown in Figure 4.7. Now the attenuation coefficient can be calculated easily. The results are shown in Figure 4.8.

The results for the plexiglas material are not surprising, the attenuation coefficient at

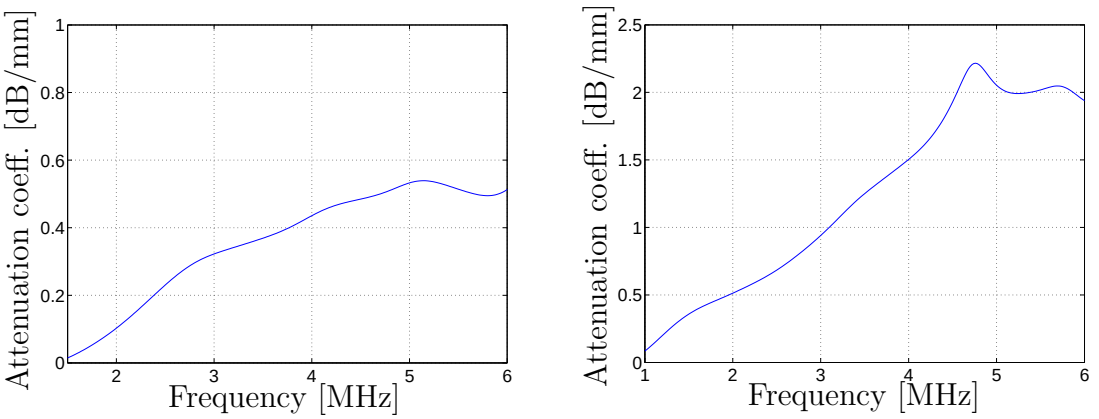

(a) Attenuation coefficient in plexiglas (b) Attenuation coefficient in polystyrene

Figure 4.8: Attenuation coefficients in polystyrene and plexiglas

5 MHz is between 0.5 dB/mm and 0.6 dB/mm, but the results for the polystyrene are completely different from the data mentioned in [11]. A reason for this discrepancy could be differences in the available polystyrene materials.

From Figure 4.8 it is clear that the attenuation coefficient at 5 MHz for the plexiglas is lower than the one for polystyrene. Therefore plexiglas is used as wedge material for the experiments which are described in the next sections.

In addition to the wedge material, the wedge design can be improved to decrease undesired reflections which could disturb the generation of the Rayleigh wave. As mentioned above, the angle θ (see Figure 4.5) can be increased slightly over 90°. Besides another angle ϑ can be introduced to decrease the propagation distance through the wedge material. Figure 4.9 shows the improved wedge design. Finally appropriate acoustic coupling plays an important role, especially using the wedge method to excite Rayleigh waves. The interfaces between transducer, wedge and specimen can be coupled using oil or glue. Usually oil is used in through-transmission measurements where a simple fixture can be designed to hold both transducers and specimen. For the wedge method both oil and glue are used and a comparison is provided in Section 5.3.2.

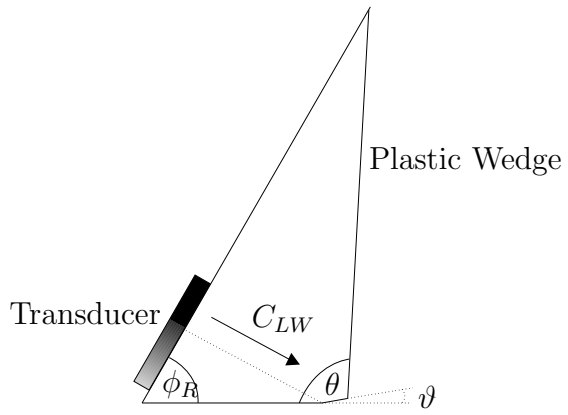

Figure 4.9: Improved wedge design

4.3.3 Critical Angle for a Nickel Base Superalloy

In this section the surface wave generation in a nickel base specimen in combination with a plexiglas wedge is presented. First of all, the longitudinal wave speed C_{LW} in the wedge material (see Figure 4.7 and 4.9) and both the longitudinal and shear wave velocities C_L and C_S in the high temperature alloy are determined experimentally.
For the wedge material, $C_{LW} = 2789\frac{m}{sec}$, and for the nickel base superalloy, $C_L = 6168\frac{m}{sec}$ and $C_S = 3307\frac{m}{sec}$, so that the Rayleigh wave speed can be computed from (2.22), hence $C_R = 3066.1\frac{m}{sec}$.
From (4.2) follows $\phi_R = 64.5°$, therefore the critical angle for the metal-plexiglas combination is determined. Now the wedge is machined carefully in order to obtain the required critical angle. Of course not only the angle itself is important, but also the quality and tolerance of the surface between the wedge and the nickel base specimen and between the transducer and wedge. Therefore these surfaces are polished carefully after machining.
Figure 4.10 shows typical incident angles (provided by the transducer company Panametrics) for the mode conversion using angle beam transducers. The angle for a Rayleigh wave excitation is approximately the same as the critical angle calculated in this section.

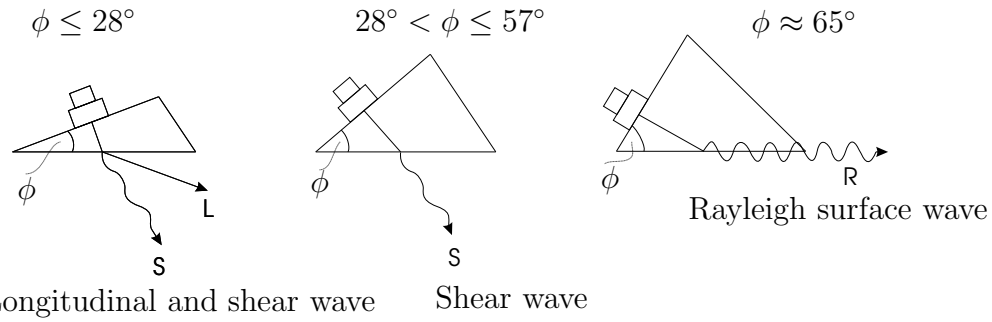

Figure 4.10: Relationship between incident angle and mode conversion using angle beam transducers

4.4 Detection System

To detect the fundamental and the second harmonic of the Rayleigh surface wave, a broadband and highly sensitive detection system is needed. In the present study, a single probe heterodyne interferometer is used.

Laser detection has several advantages compared to a detection system using a wedge-transducer combination like Barnard et al [3]. First of all, a laser detection provides absolute measurements of out-of-plane surface velocities without any of the mechanical resonance associated with piezoelectric transducers. Therefore no difficult calibration procedure is needed. Additionally, both the fundamental and the second harmonic can be measured simultaneously because of the broadband nature of the laser. With the wedge technique described in [3], one has actually two critical angles because according to Snell's law, the critical angle for measuring the second harmonic differs from the one for the fundamental. A solution to this problem could be an adjustable angle but consequently a calibration technique would be important to obtain correct results. This calibration is missing in [3]. Other advantages and also disadvantages of the laser detection system can be found in [6]. In this section the working principle of a laser detection system is described.

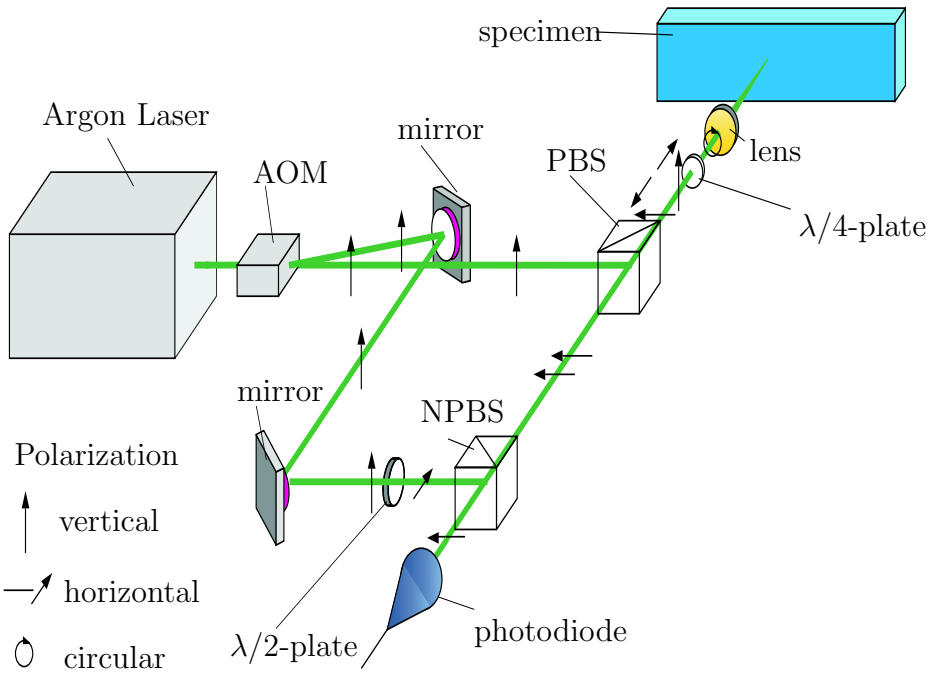

Figure 4.11: Laser Detection

4.4.1 Laser Interferometer System

The heterodyne interferometer uses the Doppler effect to determine the absolute particle velocity on the surface of the specimen. Figure 4.11 shows the experimental setup, similar to Bruttomesso et al. [6] and Hurlebaus [13] (extended to a dual probe interferometer).

The present laser interferometer works with a 2 Watt Argon Laser with a wavelength of 514nm which creates a vertically polarized light. This beam passes through an acousto-optic modulator (AOM) which splits the beam into the so called object and reference beam. Generally speaking, an AOM consists of an activated piezocrystal bonded on a quartz or Bragg cell and splits the incident beam into an infinite number of separate beams, although only the zero- and first-order beams carry about 95 % of the power from the original beam. Next to the beam splitting the AOM has another function, it shifts the frequency of either the reference beam (zero-order) or the object beam (first-order) due to the beat frequency of the piezocrystal. In the present

experiment the frequency shift of the reference beam is 40 MHz.

Now the unshifted object beam passes through a polarizing beam splitter, vertically polarized light is reflected while horizontally polarized light passes through. The reflected component travels towards the object, on the way it is circularly polarized by a $\lambda/4$-plate, focused by a lens and is reflected off the specimen or object surface. At this point the frequency of the object beam is also shifted because of the Doppler effect caused by the surface velocity. On its way back towards the photodiode, this beam is rotated from circular to horizontal polarization by the $\lambda/4$-plate, passes the PBS and hits the nonpolarized beam splitter (NPBS).

Now the way of the reference beam is described. After reflecting at two mirrors, a $\lambda/2$-plate rotates the reference beam into 45° polarized light, which is a superposition of horizontally and vertically polarized light. Then the beam hits the NPBS where it is recombined with the object beam. After leaving the beam splitter cube, finally the intensity of the light can be converted into voltage signals by the photodiodes.

Instrumentation is used to analyze the modulation of the output signal. Using a FM discriminator, it is possible to obtain the surface velocity of the specimen. Such a FM discriminator compensates the shift due to the beat frequency mentioned above. Therefore only the frequency shift due to the Doppler effect can be determined (see Hurlebaus [13] for details). After the demodulation, the signal is low pass filtered with 10 MHz to reduce the noise level. Then the signal is discretized by an oscilloscope with a sampling frequency of 100 MHz. Via GPIB the oscilloscope is connected to a PC.

With the laser interferometer system and the equipment mentioned above, it is possible to average the signal to get a higher signal-to-noise ratio. The noise is random and because of this it cancels out if the number of averaged signals is high enough. According to [20], averaging of signals reduces the standard deviation by $\frac{\sigma=1}{\sqrt{N}}$ if uncorrelated noise is considered where N is the number of signals.

Throughout this research, 1000 signals are averaged during the acquisition with the oscilloscope, the signal-to-noise level is therefore sufficient. This is particularly important if nonlinear ultrasonic measurements are performed because the detection of higher harmonics requires a clean signal. The amplitude of higher harmonics are very low in comparison to the fundamental. If the noise level in the signal is too high, it will be impossible to detect higher harmonics.

The amplitudes of the measured signals are given in Volts whereas the laser detection is based on the surface velocity. The relationship between the voltage and the velocity is given by

$$v = \frac{\lambda U}{2k} = 1.00078U \tag{4.3}$$

where k is a constant ($k = 0.257V/MHz$), λ is the wave length of the argon laser ($\lambda = 514.4nm$), U is the output voltage and v is the particle velocity.

In general interferometry can work with optically rough surfaces, although with much reduced sensitivity and speckle problems, therefore the specimens used in the present research are as reflective as possible and are polished if necessary.
More details about laser ultrasound can be found in [25].

4.5 Specimen

The specimens used in this research are shown in Figure 4.12. Specimen 1 and 2 have a more complicated geometry than specimen 3 and 4 which are essentially rectangular bars. The sample thickness is the same (t=4.7 mm).
The material is a nickel base superalloy and has superior strength at high temperatures. Therefore it is typically used in hot sections of gas turbines, rocket engines or nuclear reactors. Nickel base superalloys were developed in the early 1960's and had their first applications in cast or powder metallurgy forms. Next to the remarkable

chemical and structural homogeneity, it has excellent strength and toughness properties but poorer creep capability which restricts applications at highest temperatures. Nowadays these alloys can be found in jet engines operating in the intermediate temperature regime.

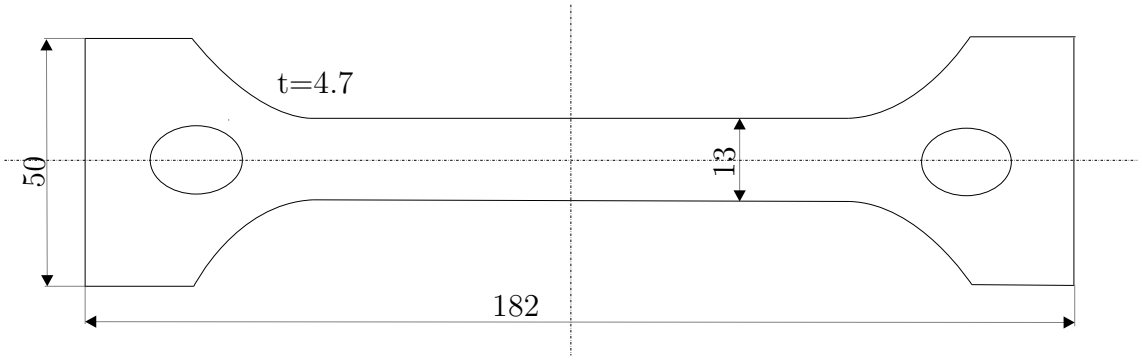

(a) Specimen 1 and 2

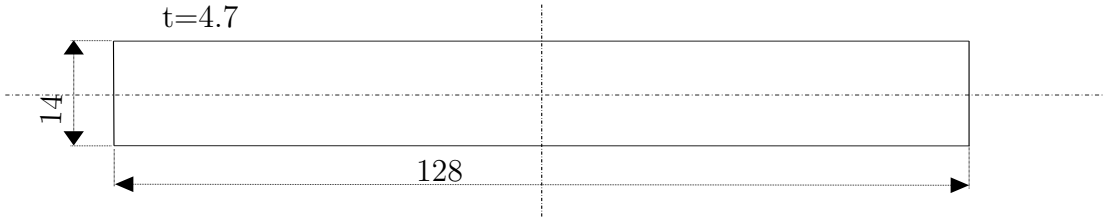

(b) Specimen 3, 4 and 5

Figure 4.12: Geometry of the specimens. Measures are given in mm

The attenuation in this material is very small and can therefore be neglected. Otherwise attenuation would be competitive to the cumulative measurement of the second order harmonic. One can say that this material is naturally very linear and homogeneous, a detection of higher harmonics is considered as a difficult task.
Table 4.1 provides material properties of the described superalloy.

Table 4.1: Material properties of a nickel base superalloy

Material	$\rho[\frac{kg}{m^3}]$	c_{L} $[\frac{m}{s}]$	c_{T} $[\frac{m}{s}]$	$E[GPA]$	ν	$\sigma_y[MPa]$
Nickel base superalloy	7861	6168	3307	213.65	0.298	1041.1

Table 4.2: Specimens with varying surface conditions used in this research

Sample:	***Surface condition***:	***Test***:
Specimen 1	Machined	Higher harmonics vs. propagation distance
Specimen 2a	Sanded, lapped	Higher harmonics vs. propagation distance Investigation of a damaged sample
Specimen 2b	Sanded, lapped, oxidized	Comparison of oxidized and unoxidized surfaces
Specimen 3	Lapped, polished	Investigation of different damage states
Specimen 4	Lapped, polished	High-cycle fatigue test
Specimen 5	Lapped, polished	Low-cycle fatigue test

The two specimens shown in Figure 4.12 are used in different sets of measurements with varying surface conditions. Table 4.2 summarizes and labels the different samples to avoid confusion later in this research.

CHAPTER V

EXPERIMENTAL RESULTS - QUANTIFICATION OF SYSTEM PERFORMANCE AND NONLINEARITY

The experimental generation and detection of a Rayleigh wave is described in the first section. Moreover different frequencies and different input signals are considered. Signal processing and the definition of higher harmonics in Rayleigh waves are provided in Section 5.2. Improvements and changes in the wedge design are emphasized in Section 5.3. Besides different coupling methods for the interface between wedge and specimen are investigated.

The last section of this chapter deals with nonlinear ultrasonic measurements. Several sets of experiments are described, and the propagation distance of the Rayleigh wave along the surface of the specimen is changed. Both the conventional setup #1 and the improved setup #2 are used and compared.

5.1 Generation and Detection of a Rayleigh Wave

As described in Section 4.3, the generation of a Rayleigh surface wave is realized with the wedge method where a plastic wedge with a critical angle is used to convert a longitudinal wave propagating through the plastic material into a surface wave. Details about the experimental setup can be found in Section 4.1 and 4.2, setup #1 is used for this set of measurements. Figure 5.1 shows a typical signal in the time domain. The amplitude is directly related to the out-of-plane surface velocity and is given in Volts. A 5-cycle, toneburst signal is used to drive the 5 MHz transducer.

The signal is amplified with a 50 dB high voltage amplifier. As mentioned earlier, the input voltage for this amplifier should not exceed 1 V. In most of the experiments, an input voltage of 800 mV is used, hence the input signal is amplified to 253 V. Of course, not the whole voltage drives the transducer, but losses in the electrical circuit are hard to quantify.

The sinusoidal toneburst signal is detected with the laser interferometer system described in Section 4.4. In this case a 3 MHz input frequency is used because the ultrasonic transducer used in this experiment has a resonance frequency of about 3 MHz, therefore the peak-to-peak amplitude is expected to be at a maximum at 3 MHz. Note that this input is only used to detect and identify the arrival of the Rayleigh waves.

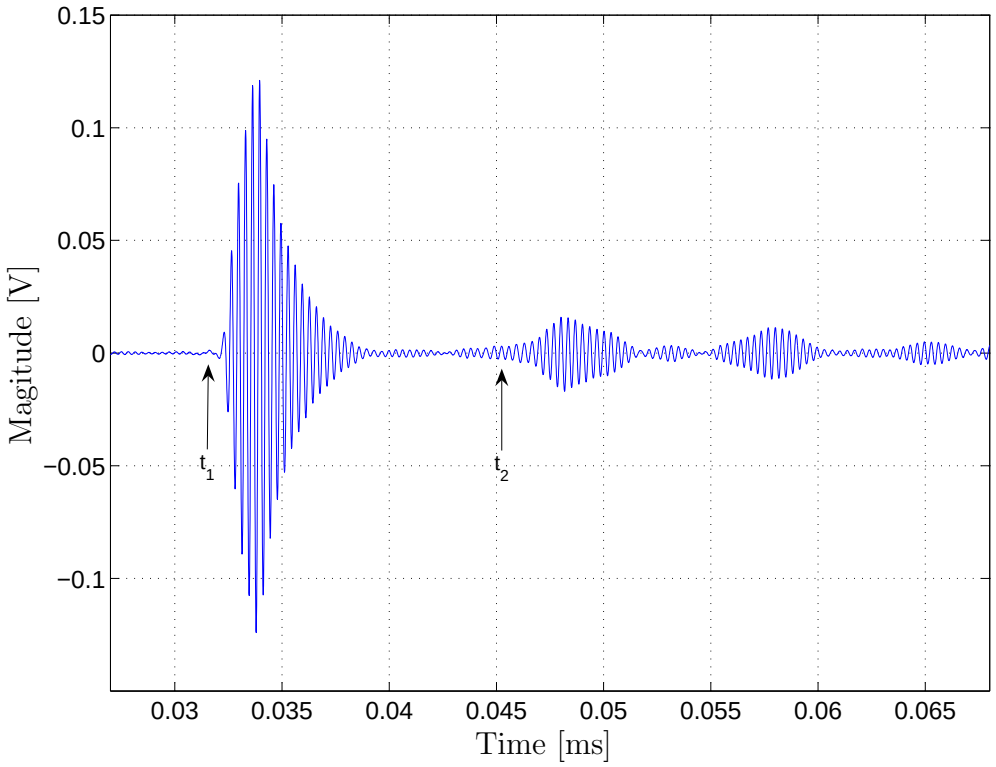

Figure 5.1: Time signal for a toneburst with 5 cycles and 3 MHz

Figure 5.1 shows the arrival of the detected signal of the input sinusoidal wave at

slightly more than 3 ms (t_1 in Figure 5.1). The question is now if this measured peak is a Rayleigh wave. Because both the propagation distance and the Rayleigh wave speed in the material of the specimen are known (see section 4.3.3), one can estimate the arrival time of the toneburst signal. First of all the propagation distance of the longitudinal wave in the wedge material is 2.8 cm, then this longitudinal wave converts into a Rayleigh wave and propagates 7 cm along the surface until it reaches the detection point. The estimated arrival time of the toneburst signal is therefore

$$t = t_L + t_R = \frac{0.028m}{2789\frac{m}{s}} + \frac{0.07m}{3066\frac{m}{s}} = 0.033ms. \tag{5.1}$$

This result is consistent with the measured arrival time in Figure 5.1. A slight time delay of the sinusoidal wave is expected because of the interface between the wedge and specimen, but all in all, it is clear that a Rayleigh wave propagates with this wedge design. The smaller peaks at later arrival times might be reflections off the hole and the free end of the specimen, the geometry of the sample (Specimen 1) can be found in Figure 4.12. The first reflection occurs at time t_2. From Figure 5.1, it is obvious that this reflection does not affect the toneburst signal starting at time t_1. As long as the toneburst signal of interest is between t_1 and t_2, geometrical effects can be neglected.

Other wave propagation possibilities are longitudinal and shear waves which travel with a different wave speed. Because laser detection is used, one can only measure out-of-plane waves, therefore only longitudinal and SV waves are possible. As mentioned in Section 4.3.3, the shear wave speed is higher than the one of the Rayleigh wave meaning that SV waves would arrive earlier than the wave measured in this experiment. The other possibility is that a longitudinal wave goes straight through the material of the specimen and reflections at the other side or wall of the relatively thin specimen would occur (skip effect) but even then the arrival of the sinusoidal wave would be a lot earlier because the wave speed of the longitudinal wave is about two times higher than the Rayleigh wave speed. The estimated arrival time would be

0.02 ms.

5.1.1 Frequency

From (3.18), one can see that the amplitude of the second harmonic depends on the frequency, the relation is even quadratic, meaning that the magnitude of the second harmonic increases with a higher frequency. In the literature one often find experiments with a 5 MHz input signal to detect the second harmonic at 10 MHz and so on. Barnard et al. [3] and Blackshire et al. [5] for instance use this frequency for similar measurements. The laser detection system of the present research is linear up to 10 MHz [13], therefore the limit for the input frequency is about 5 MHz.

Using the same setup as in the preceding section, the amplitude of the signal decreases for a higher frequency. This is because the driving frequency is not the resonance frequency of the transducer anymore. For nonlinear measurements it is quite important to increase the frequency though because if the amplitude of higher harmonics is too low, the information will disappear below the noise level.

Because information at higher frequencies are considered, the low-pass filter of the laser detection system is changed from a 10 MHz to a 20 MHz filter. All the following plots show input signals with a frequency of 5 MHz. Moreover the number of cycles is increased from 5 to 25 cycles, details about different number of cycles can be found in Section 5.3.3. Figure 5.2 shows a typical signal with a frequency of 5 MHz and 25 cycles.

Of course the sample thickness plays also an important role because the theoretical derivations of Rayleigh waves are based on an elastic half space and the specimen used at the measurements is relatively thin. As mentioned in Section 2.3, the relative displacements vanish if the distance from the free surface of the specimen is high in comparison to the wavelength. The sample thickness is 4.73 mm, the wavelength can

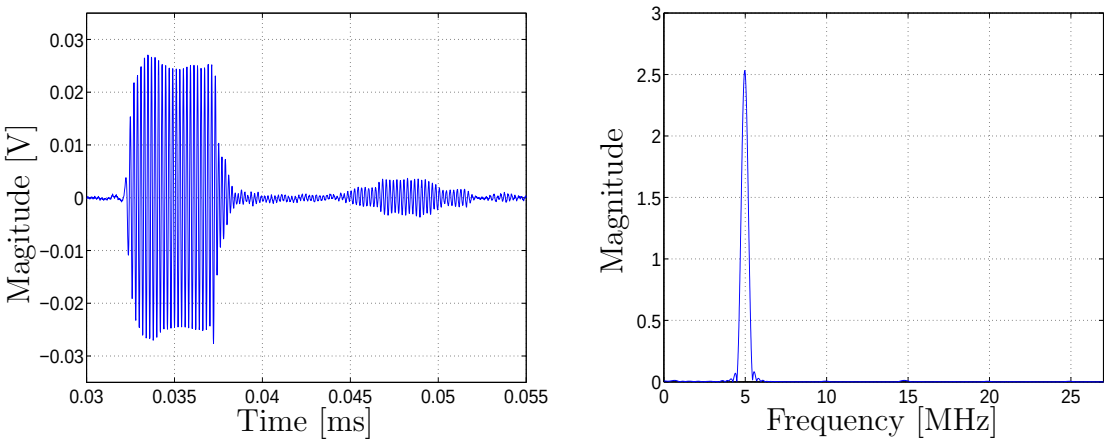

(a) Time Domain (b) Frequency Domain

Figure 5.2: Time signal and FFT of a toneburst signal with 25 cycles and 5 MHz

be calculated from

$$\lambda = \frac{C_R}{f}. \tag{5.2}$$

For a frequency of 5 MHz, the wavelength is therefore 0.613 mm. This result means that the sample thickness is almost eight times higher than the wavelength. Even for a frequency of 3 MHz the sample thickness is still four times higher than the wavelength. It can be assumed that theoretically almost no displacement can be observed at the bottom of the specimen meaning that the Rayleigh wave is not disturbed by these displacements or reflections from the other surface. Otherwise a Lamb wave would be generated instead of a Rayleigh wave.

5.2 Signal Processing and Definition of Higher Harmonics

To detect higher order harmonics it is important to do signal processing. A Discrete Fourier Transform (DFT) or a Fast Fourier Transform (FFT) is necessary to separate the small higher order harmonics from the fundamental wave in the frequency domain.

To make sure that only the steady-state part of the toneburst signal is used, a very

careful windowing (Hanning window, see Figure 5.3 showing a typical time signal measured with setup #2) is applied to the time signal. Only the datapoints within

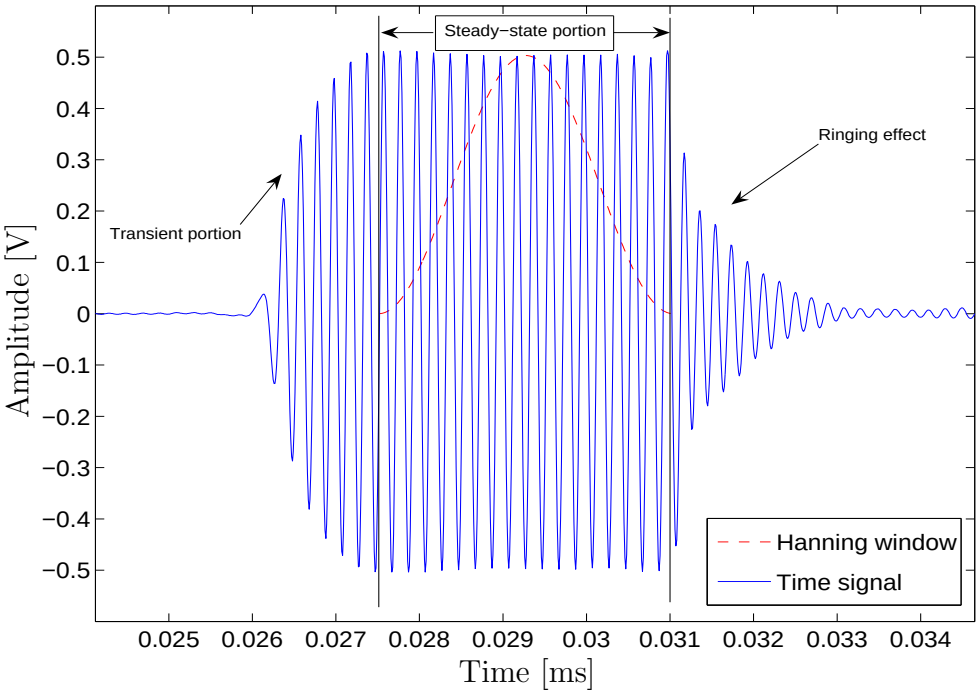

Figure 5.3: Time signal with applied Hanning window

the steady-state part are selected and then transformed in the frequency domain where the information about higher harmonics becomes visible.

The use of a Hanning window gives the best results because of the lowest numerical noise, suppression of side lobes and a stable signal containing many cycles, thus there is no risk to cut off important information from the beginning or the end of the window. With a rectangular window higher harmonics seem to be hidden under the noise level. Details about toneburst signals and the number of cycles can be found in Section 5.3.3. For a long steady-state part of the signal, the resolution turns out to be good enough. Of course, the resolution in the frequency domain would be better if the window is taken over the whole signal but for the present research it is more

convenient to select only the toneburst signal, then a comparison between different samples and propagation distances is allowed.
More details about signal processing can be found in [17] and [20].

As mentioned above, one can see the higher harmonics in the frequency domain. To allow a comparison between different propagation distances and samples, the magnitude of the FFT is normalized meaning that the magnitude of the fundamental is always 1. Figure 5.4 shows the proposed normalization procedure for the magnitudes of higher harmonics. First, the absolute values in the frequency domain are considered and the peak at the fundamental frequency is named as A_1', whereas the absolute amplitude of the 2nd harmonic is called A_2'. The harmonic ratio or β' is defined as $A_2'/(A_1')^2$. Now one can normalize these absolute values with respect to the amplitude of the fundamental frequency.

5.3 Improvements and Specifications for the Generation of Rayleigh Waves

Possible improvements for efficient Rayleigh wave generation are carried out in this section. The experimental setup #1 is used to investigate changes in wedge designs (Section 5.3.1), couplants (Section 5.3.2) and different number of cycles (section 5.3.3). Plots are provided in each section to show how the amplitude of the measured time-signal changes.

5.3.1 Different Wedge Designs

The amplitude of the detected signal can be increased using an improved wedge design. Details about the wedge design are mentioned earlier in Section 4.3.2. Especially a smooth and flat wedge surface which is attached on the specimen shows a lot of improvement, the amplitude of the signal increases considerably (when compared to Figure 5.2, for example), Figure 5.5 shows the result.

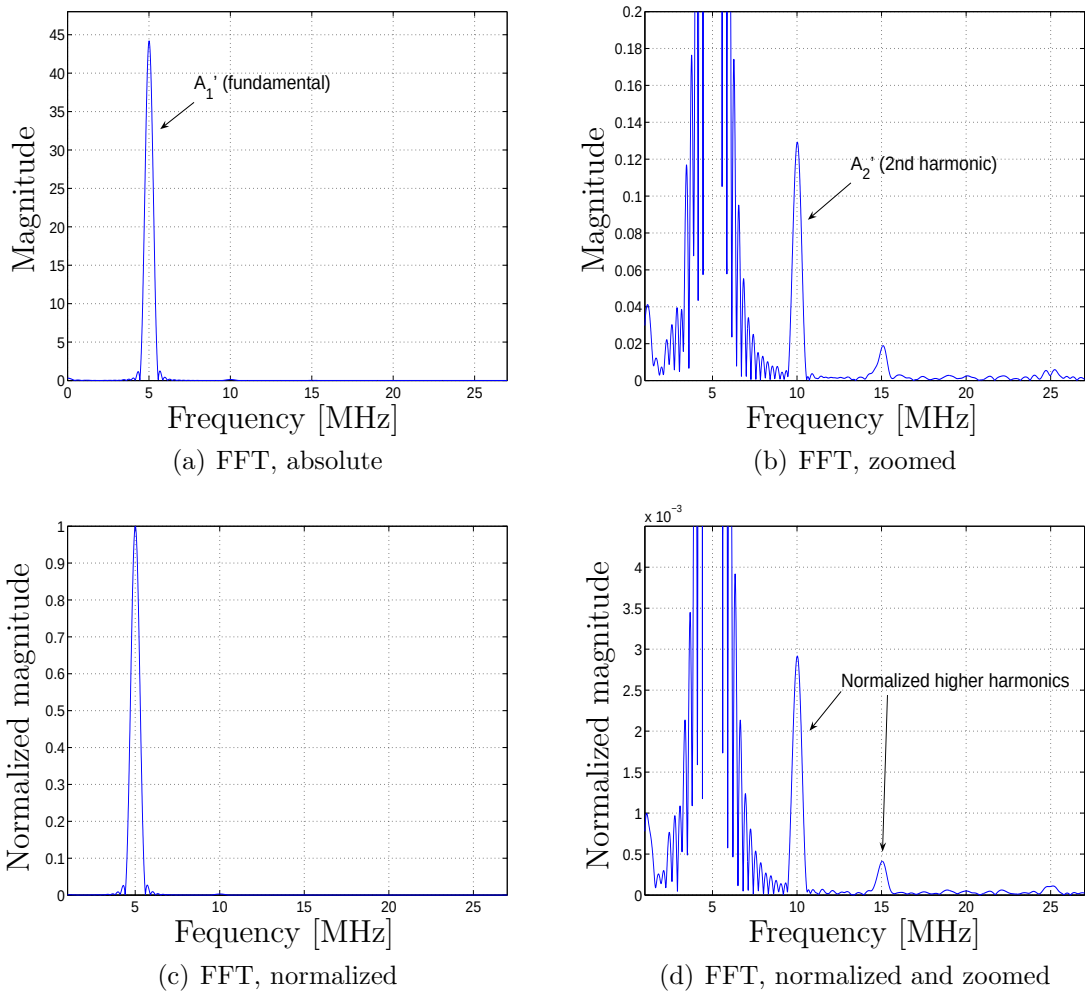

(a) FFT, absolute

(b) FFT, zoomed

(c) FFT, normalized

(d) FFT, normalized and zoomed

Figure 5.4: Frequency domain including the absolute and normalized values of the fundamental and higher harmonics

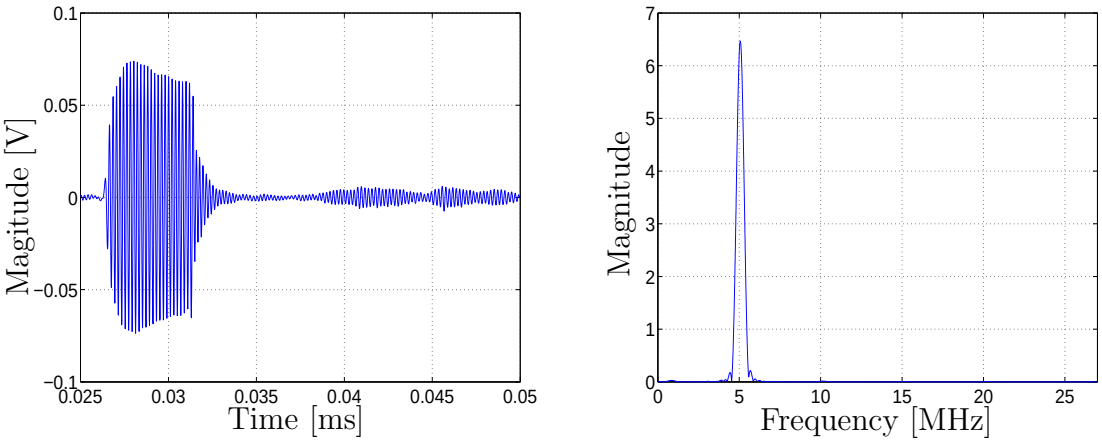

(a) Time Domain (b) Frequency Domain

Figure 5.5: Time signal and FFT of a toneburst signal with 25 cycles, 5 MHz and an improved wedge design

Moreover the area or especially the length of this interface is increased, and in addition to that, the glue is used more carefully to get an improved coupling at the interface between wedge and specimen.

5.3.2 Coupling

In general a couplant is a material that facilitates the transmission of ultrasonic energy if an interface exists. Because of the acoustic impedance mismatch between air and solids (like the test specimen or the wedge), nearly all of the energy is reflected and very little is transmitted into the test material. The couplant displaces the air and makes it possible to get more sound energy into the specimen so that a usable ultrasonic signal can be obtained. A thin film of oil, glycerin or water (fluid coupling), or glue is used at the interfaces in contact ultrasonic testing.

The interface between the wedge and the steel specimen is a highly sensitive part of wave propagation. Of course there are different losses and even scattering, so it is very hard to predict or model the wave propagation at this interface.

Cement glue has the advantage that no additional fixture is needed to hold the wedge, therefore the position of specimen and wedge can be varied without problems. Besides

the glue is a reliable coupling once it is fixed. All the measurements so far were conducted using cement glue.

The disadvantage of this glue is that not the whole interface is coupled properly, you can see several scatterers or even air bubbles on the side after the glue is hardened. Especially if one wants to replace the glue or change the wedge position, a completely new interface is created, comparisons between different sets of experiments seem to be difficult, although this glue is still a convenient and cheap way to attach the plastic wedge on the steel specimen.

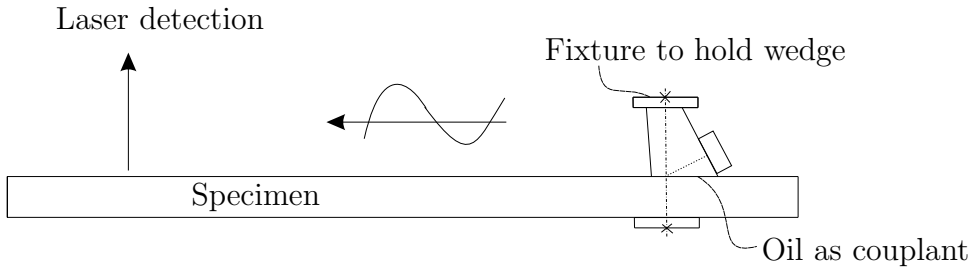

Figure 5.6: Fixture to hold wedge on specimen using oil as couplant

To avoid the problems mentioned above, oil can be used as couplant. Of course, a fixture is needed to hold the wedge firmly, although this fixture is not complicated if the wedge is cut so that two parallel surfaces are created. Figure 5.6 shows such a fixture where basically two plates are pressed on the wedge and specimen. Now a clean and pure interface can be seen, no scatterers or air bubbles disturb the wave propagation. The signal of the improved setup can be seen in Figure 5.7. The amplitude increases again, besides it is easier to change the wedge position along the specimen which is a big advantage, especially for measurements with different propagation distances.

Another interface exists between the plastic wedge and the ultrasonic transducer which is bonded on the sloping surface of the wedge. A fixture which could hold the transducer would be very complicated to realize, oil as coupling is therefore not practical. In this case the cement glue mentioned above seems to be the best way to

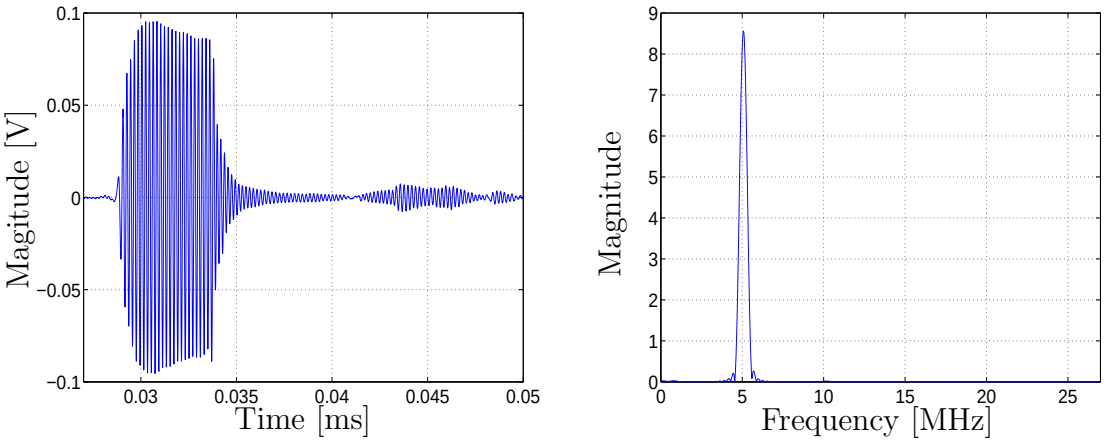

(a) Time Domain (b) Frequency Domain

Figure 5.7: Time signal and FFT of a toneburst signal with 25 cycles, 5 MHz and an improved coupling using oil and a fixture (compared to Figure 5.5)

get an appropriate coupling. Because the transducer stays the same for different sets of measurements, there is no need to replace the transducer or the position, therefore it is convenient to use glue as couplant.

5.3.3 Number of Cycles

With the function generator, almost any desired number of sinusoidal cycles can be generated, so this section provides a comparison between different number of cycles. Figures 5.8 and 5.9 show a zoomed portion of the time signal, these plots come from the same experiment, only the number of the cycles is changed from 5 to 25.

One can usually distinguish three different parts of the detected toneburst signal: A transient part can be seen at the beginning of the signal, the frequency of this portion depends on the properties of the ultrasonic transducer. With the present transducer the frequency of the transient part is about 3 MHz which seems to be the same as the resonance frequency. This frequency remains constant, even if the driving frequency of the transducer is changed.

The second portion of the detected signal is the so called steady-state part where the frequency is the same as the driving frequency of the transducer. This is the real

signal where all the information is saved and used to calculate the magnitudes of the higher harmonics.

The last portion of the signal consists of ringing effects. Because the piezoelectric transducer is a mechanical system, vibrations occur which result in an exponential decay of the amplitude. Of course these ringing effects are not desirable, but in comparison to the steady-state portion of the signal, the magnitude is relatively small.

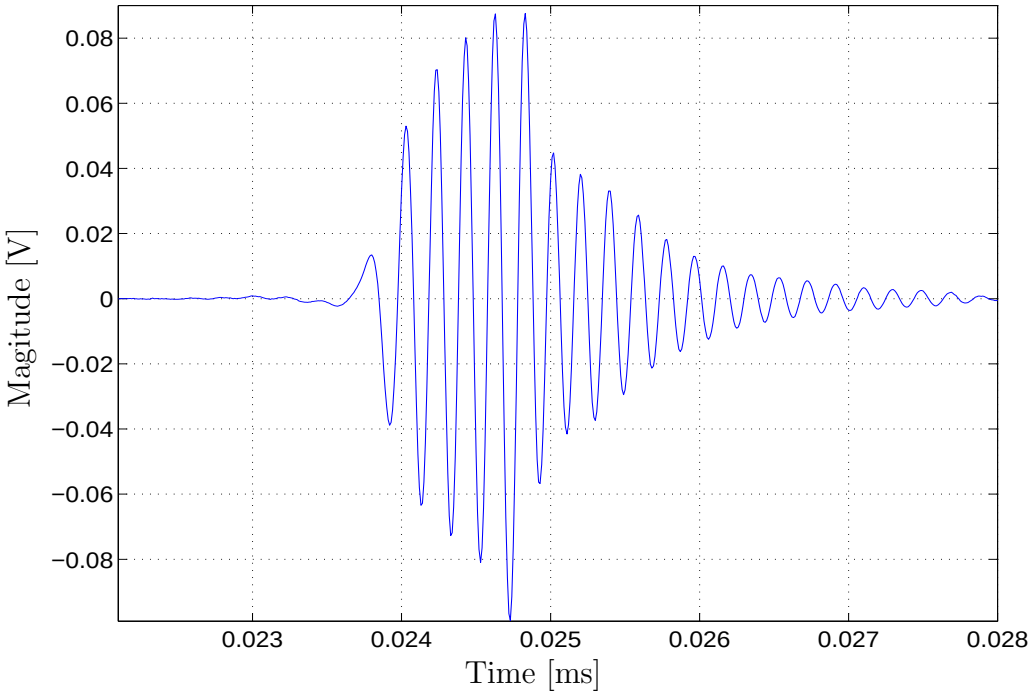

Figure 5.8: Toneburst with 5 cycles

Figure 5.8 shows a typical signal of a toneburst with 5 cycles. It can be seen readily that the transient and ringing part of the signal are relatively high where the steady state part is still visible but small. A toneburst signal with 25 cycles can be found in Figure 5.9. The steady state part of the signal is dominant, therefore it is relatively easy to window this particular part of the signal which makes the signal processing easier. Moreover the driving frequency of the transducer is dominant in comparison

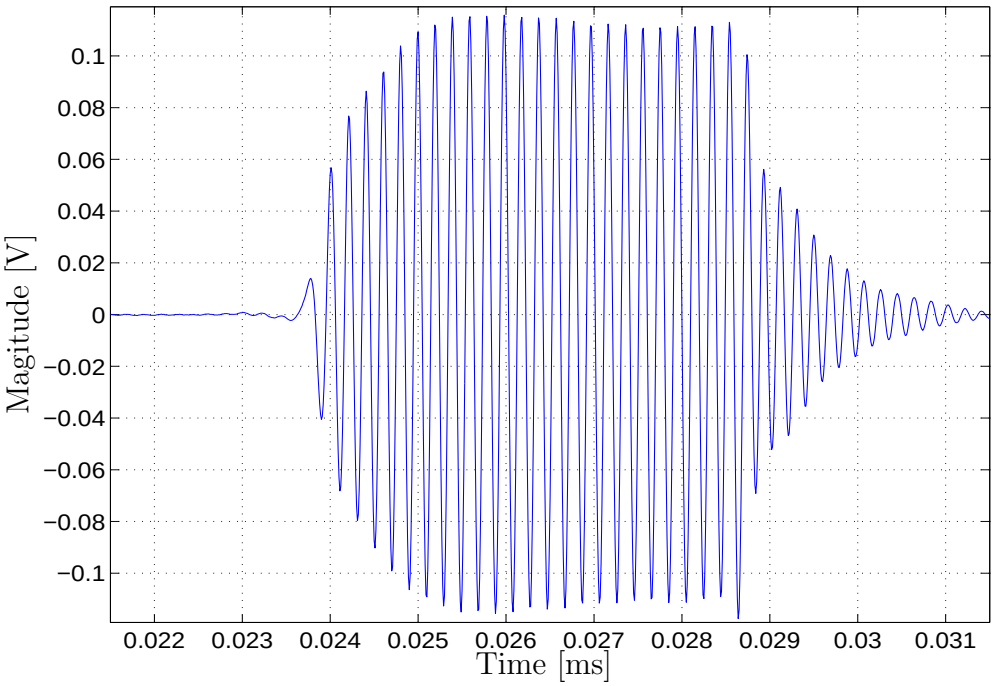

Figure 5.9: Toneburst with 25 cycles

to the frequency of the transient part.

All in all 25 cycles appear to be a sufficient number of cycles. This is also the number Blackshire et al. [5] are using in similar experiments.

The improvements mentioned above lead to a peak-to-peak amplitude of about 0.2 V using the experimental setup #1, which is still not very high, but with respect to the peak-to-peak amplitude without these improvements (see figure 5.2), an increase of 400 % could be achieved.

5.4 Amplitude of the Fundamental and Generation of a Plane Wave

Applying all the improvements described in the previous sections and using the experimental setup #2, a peak-to-peak voltage in the time-domain signal of about 1

V is achieved which is considered as very high with respect to the sensitive point-like laser detection system used in this research. Of course the Ritec amplifier of setup #2 is the reason for this big increase in the amplitudes. With the conventional amplifier, a voltage up to 0.25 V (peak-to-peak) was measured. Figure 5.10 compares the maximum amplitude for each of the two experimental setups. The Rayleigh wave propagation distance is 6.5 cm for setup #1 and 4.7 cm for setup #2. Another interesting feature is that the output voltages stay about constant for the

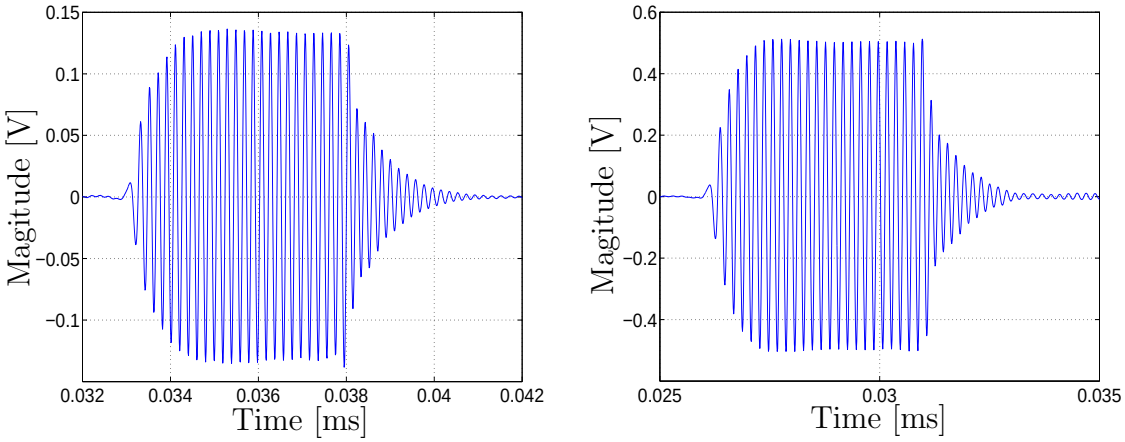

(a) Time Domain, Setup #1

(b) Time Domain, Setup #2

Figure 5.10: Maximum amplitude for each of the two experimental setups

different propagation distances meaning that there is no geometrical spreading (the amplitude would decrease with propagation distance with the factor of $\sqrt{r}$, where r is the propagation distance) visible using the experimental setup #2. This observation means that a plane Rayleigh surface wave is generated. Figure 5.11 shows the almost constant magnitude of the peak-to-peak voltage from the time signal.

With the conventional experimental setup (setup #1) it was not clear if a plane wave is generated or if geometrical spreading or even geometrical effects occur. The improved experimental setup (setup #2) solves this problem or uncertainty, therefore a reliable comparison between different propagation distances and damage states with respect to nonlinear wave propagation and higher harmonics is allowed .

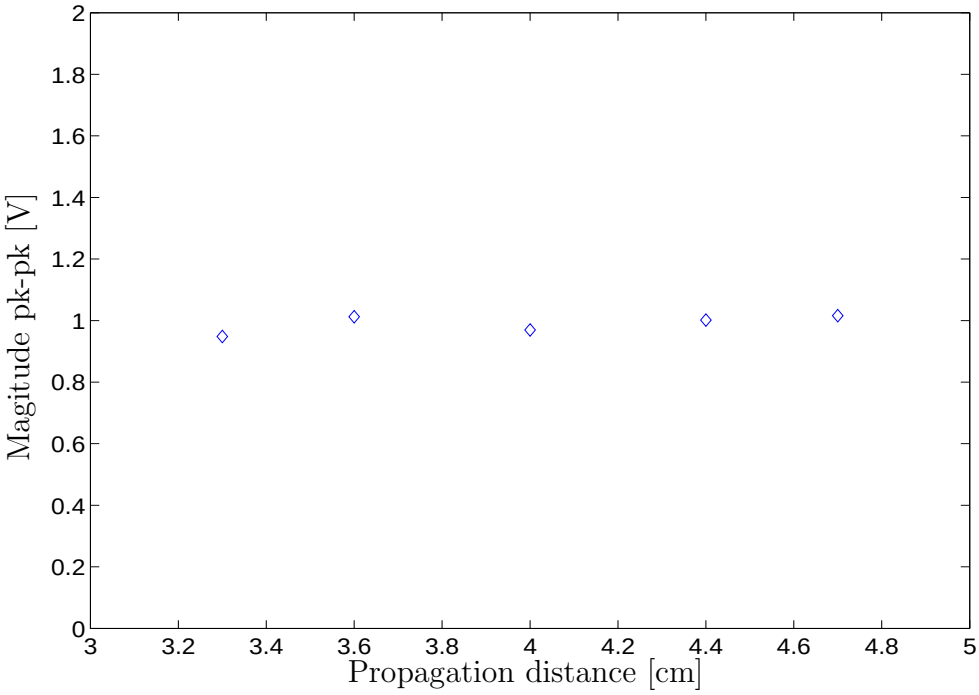

Figure 5.11: Peak-to-peak voltage from the time signal for different propagation distances

With the maximum peak-to-peak voltage of 1 V and all the improvements mentioned above, it is possible to start looking at higher harmonics and nonlinear wave propagation. Especially the experimental setup #2 has the potential to enable nonlinear acoustic measurements.

5.5 Dependence of Higher Harmonics on Propagation Distance

The following sections describe measurements and experimental results of nonlinear wave propagation, the theoretical background is provided in chapter 3. As one can see from (3.18), the amplitude of the second harmonic depends on the propagation distance, and the relation is linear. Moreover the amplitude ratio $\frac{A_2}{A_1^2}$ is proportional to the dimensionless nonlinearity parameter β and should be an indicator of material

nonlinearity for a certain specimen. This section describes the experimental detection of the second harmonic and its relation to the propagation distance. Details about the specimen and its properties can be found in Section 4.5, Specimen 1 is used in the following.

The experimental setup used in this first set of measurements is explained in Section 4.2, this setup is referred as the improved setup #2 in the following. A toneburst with 25 cycles and an input voltage of 1.12 V is generated by a function generator, afterwards this sinusoidal signal is amplified with a gated high power amplifier and drives the ultrasonic transducer with 5 MHz. The transducer is attached on the sloping surface of a plastic wedge which was machined in a way that a Rayleigh surface wave is excited propagating along the surface of the nickel base superalloy sample. The wedge is attached on the specimen using a fixture and oil as couplant. The detection side consists of the laser interferometer system explained in section 4.4.

As mentioned in section 4.4, 1000 signals are averaged to get a high signal-to-noise ratio (SNR). Because the amplitudes of the higher harmonics are very small in comparison to the fundamental, a clean signal in the time domain is needed.

The dependence of higher harmonics on propagation distance is the most reliable way but also the most difficult way to measure nonlinearity in a certain specimen and an indicator if the experimental system works properly. To ensure that the higher harmonics are not generated by the experimental system itself, one has to test the system linearity and the repeatability of the experimental procedure.

5.5.1 System Linearity

To check the system linearity, one can change the input voltage and detect the fundamental and second harmonic using the same specimen, the same propagation distance

and experimental setup to make sure that the measured higher harmonics are an indicator of material nonlinearity and not spurious nonlinearity due to the instrumentation. To sum up one can say that quadratic-type material nonlinearity is measured while system linearity is proven indirectly.

In this case the input drive level varies from 1.05 V to 1.13 V (this is the voltage before amplification). If the experimental setup is linear, one will see a linear relationship between the amplitude of the 2nd harmonic A_2' (which is the transformed amplitude of the FFT algorithm, see figure 5.4 for further explanations) and the squared amplitude of the fundamental $A_1'^2$. Figure 5.12 shows such a plot for a Rayleigh wave propagation distance of 4.7 cm using Specimen 1. A linear relationship is clearly visible for different input voltages.

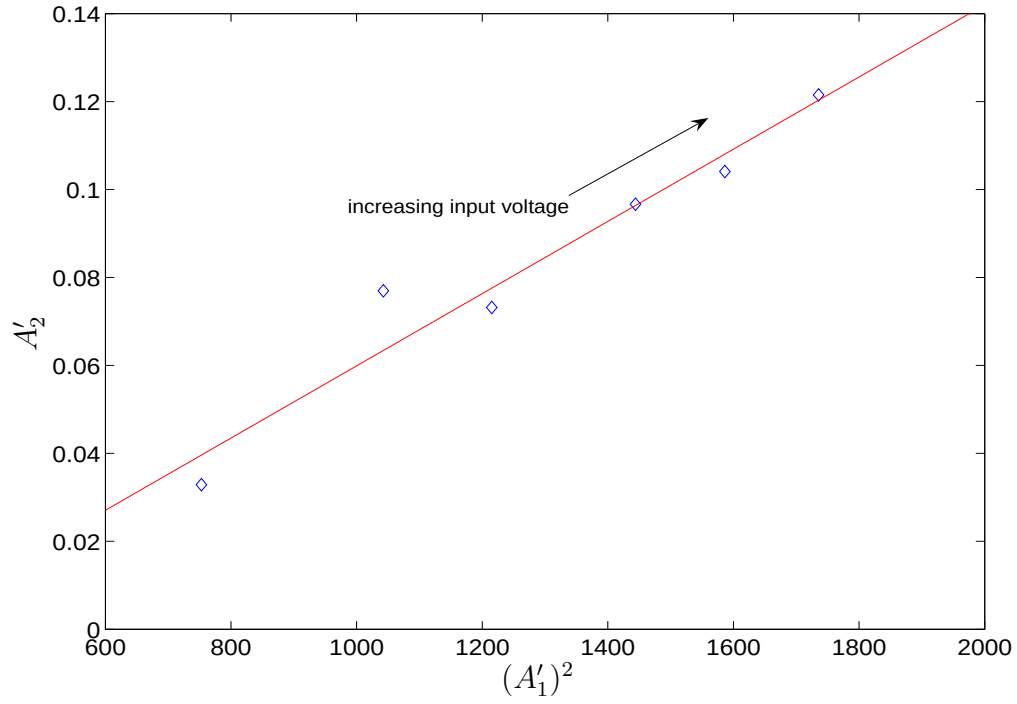

Figure 5.12: System linearity for the improved experimental setup (setup #2)

One can see that the system is linear especially for higher input voltages. To obtain

the highest possible amplitude and a linear electrical circuit, the measurements described in the following pages are conducted with an input voltage of 1.12 V. The limit of the Ritec high power amplifier is around 1.14 V.

5.5.2 Repeatability

Because interfaces are involved in these ultrasonic measurements, one has to investigate if these interfaces contribute to the measured nonlinearity and if a repeatability of the measurements can be achieved. To gain information about the influence of the interface-changes between wedge and specimen, one can conduct a simple experiment where the wedge and couplant are removed, attached again and the measurements are repeated. Figure 5.13 shows the linear relation between A_2' and $(A_1')^2$ for the two measurements. Of course the propagation distance is kept constant (4cm) and

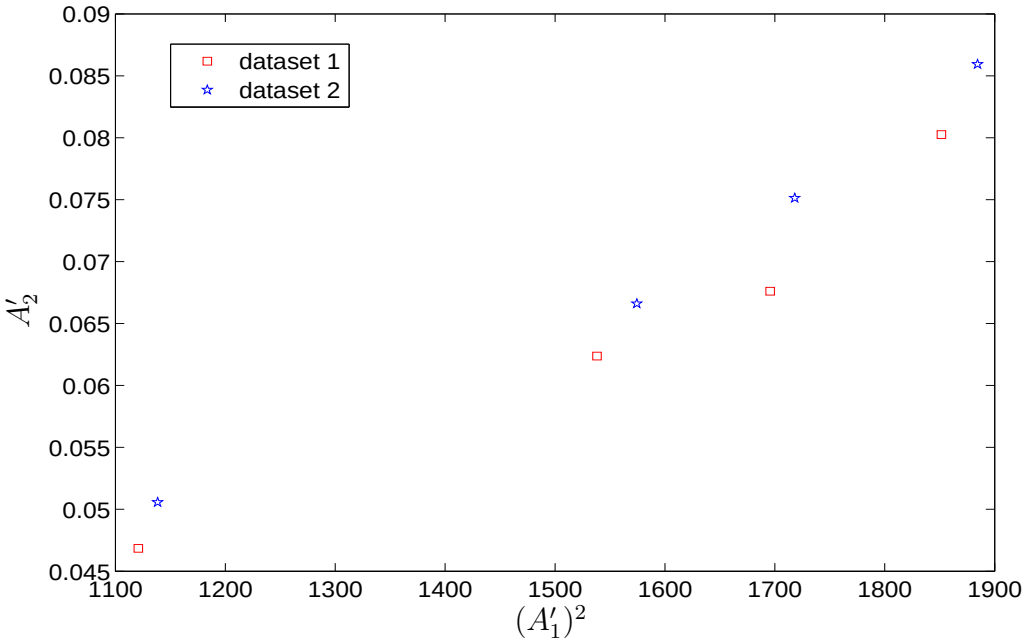

Figure 5.13: System linearity and repeatability for two different datasets with the same propagation distance using setup #2

different input voltages are used. One can see at the plot that the slope for the two

different datasets is nearly constant meaning that the measurements are repeatable and that the replacement of the wedge and couplant has no dominant influence on the results.

5.5.3 Nonlinear Ultrasonic Measurements

Now the influence of the propagation distance on the magnitude of the second harmonic is investigated. The propagation distance is varied from 3.3 to 4.7 cm. A fixture is designed to move the specimen together with the attached wedge in a repeatable and reliable way, so that the interface (oil as couplant) between the wedge and specimen stays the same for different propagation distances. In addition to that the alignment for the laser detection can be improved and facilitated. The results are shown in Figures 5.14, 5.15, 5.16, 5.17 and 5.18.

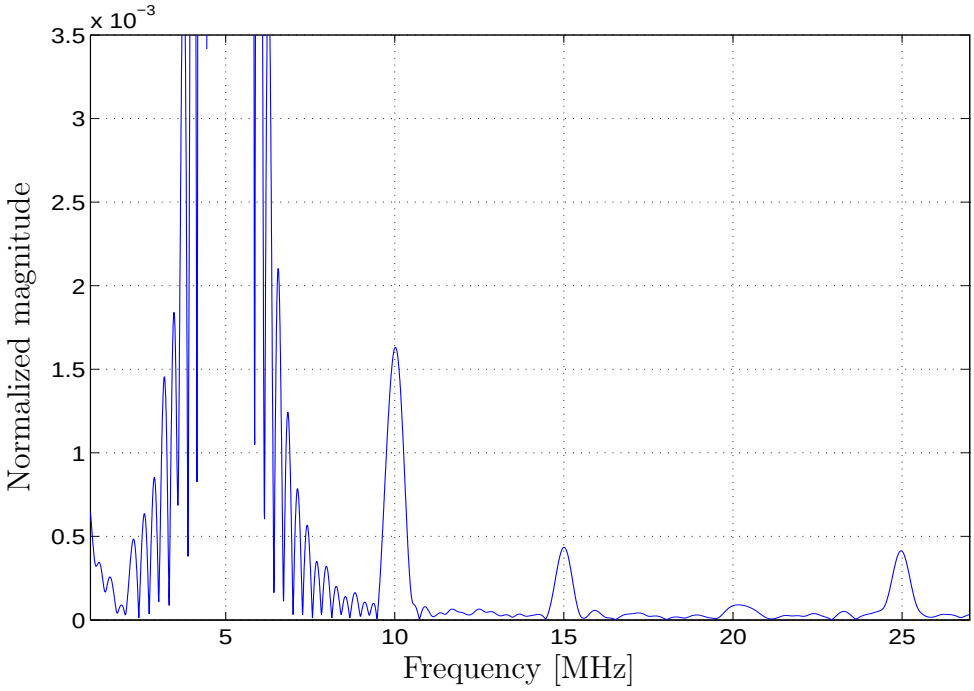

Figure 5.14: FFT of a toneburst signal with 25 cycles, 5 MHz and a propagation distance of 3.3 cm using setup #2

Figure 5.19 summarizes the results mentioned and shown above. As one can see from the linear curve fitting, it is clear that the amplitude of the second harmonic increases

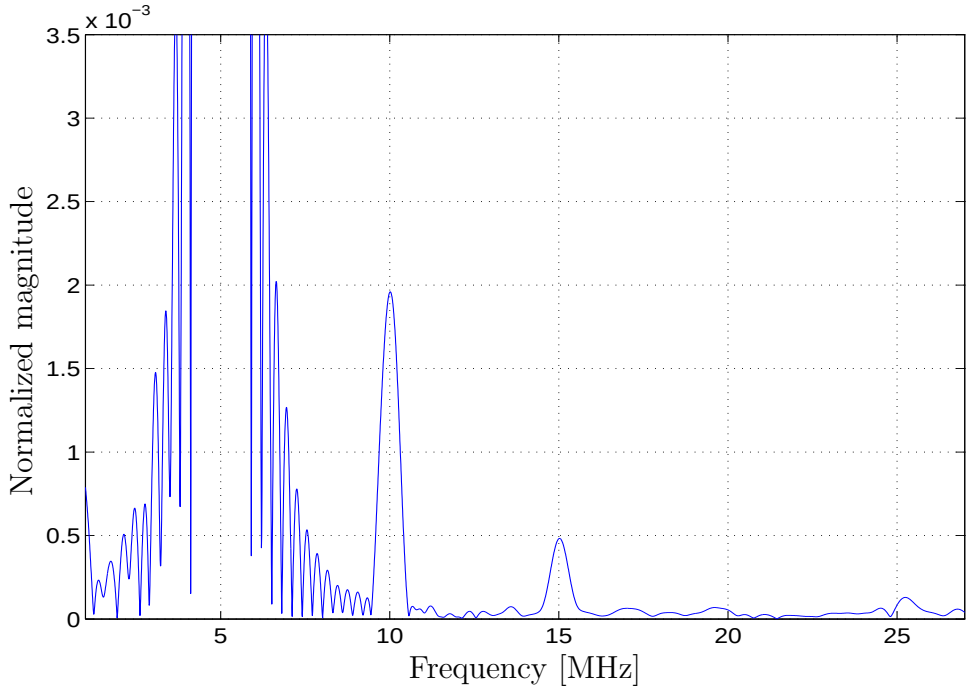

Figure 5.15: FFT of a toneburst signal with 25 cycles, 5 MHz and a propagation distance of 3.6 cm using setup #2

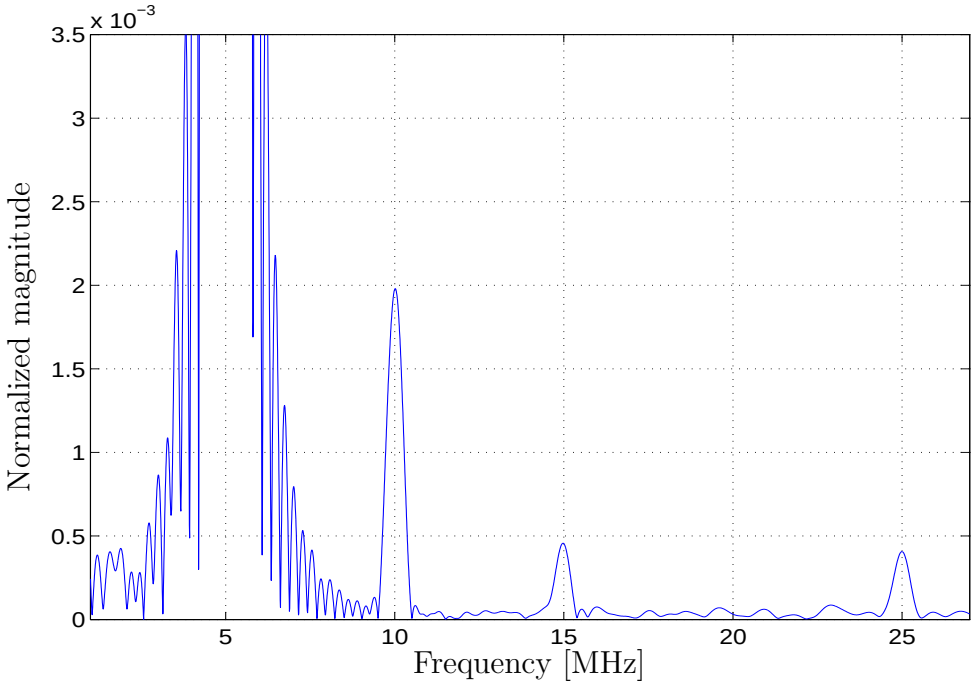

Figure 5.16: FFT of a toneburst signal with 25 cycles, 5 MHz and a propagation distance of 4 cm using setup #2

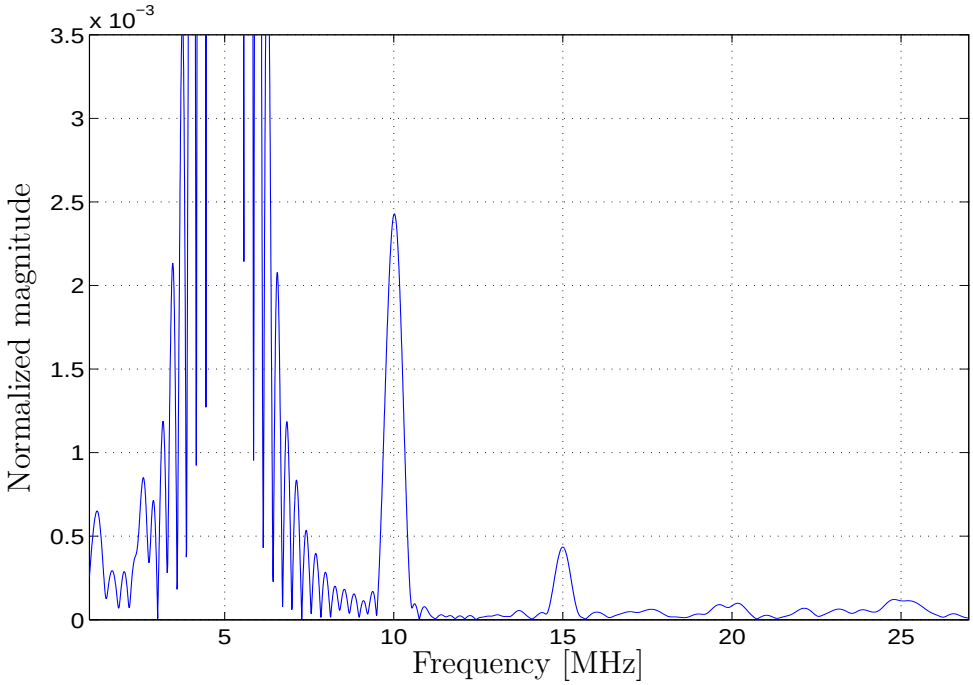

Figure 5.17: FFT of a toneburst signal with 25 cycles, 5 MHz and a propagation distance of 4.4 cm using setup #2

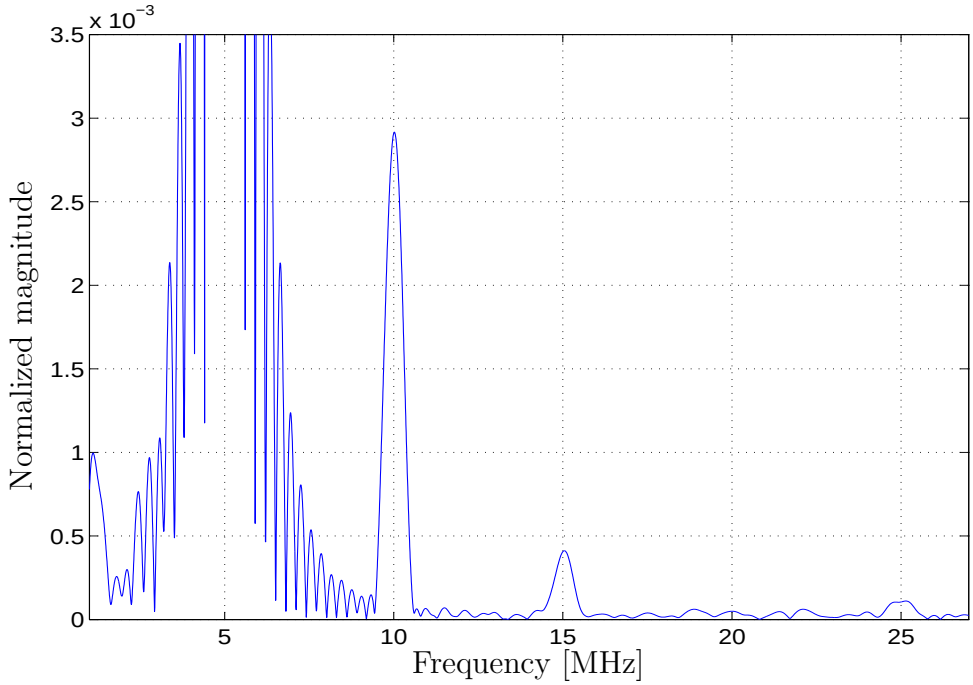

Figure 5.18: FFT of a toneburst signal with 25 cycles, 5 MHz and a propagation distance of 4.7 cm using setup #2

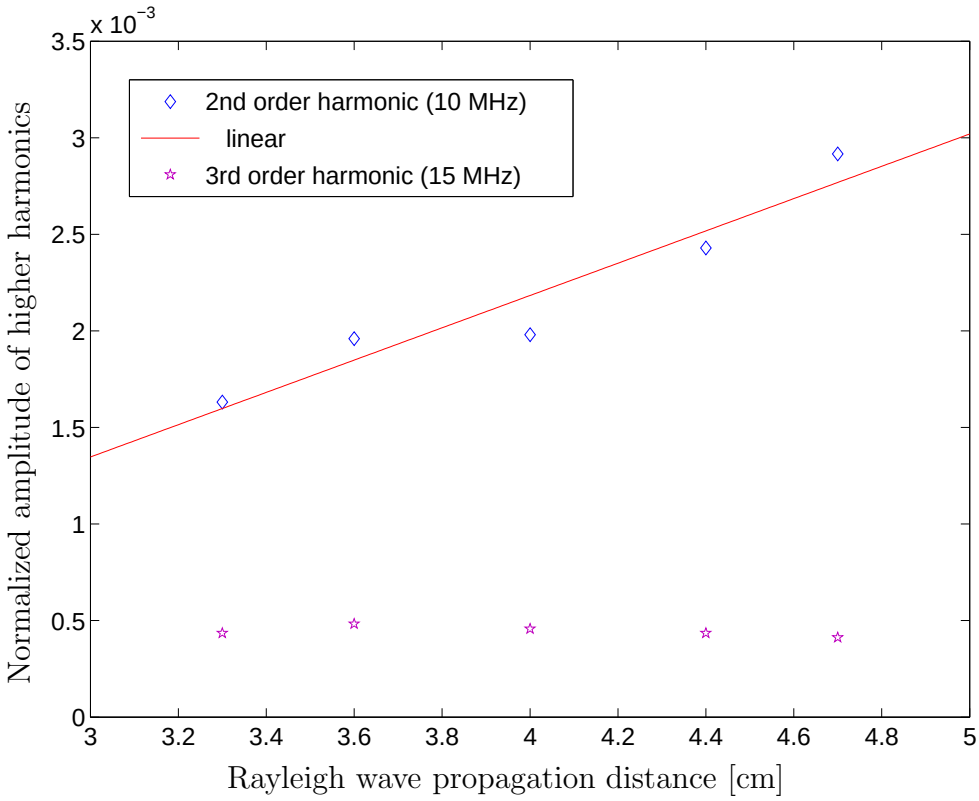

Figure 5.19: Higher harmonics over propagation distance for the improved experimental setup (setup #2)

linearly with propagation distance.

In comparison to the conventional setup, the normalized amplitudes of the second harmonic (normalized with the amplitude of the fundamental frequency) are even higher since the instrumentation has less contribution to the higher harmonic generation. The reason for this is the higher signal-to-noise ratio using the improved experimental setup, the second harmonic is well above the noise-level and can be fully detected. The increase in amplitude of the normalized second order harmonic is therefore not surprising.

The third order harmonic or rather the peak at 15 MHz is investigated as well and its amplitude stays about the same. The material induced third order harmonic seems to be well below the third order harmonic from the instrumentation, otherwise a

linear relationship between third order harmonic and propagation distance would be observed. The relatively small peaks at 15 MHz also show that the influence of the instrumentation (especially the high power amplifier) is low, a comparison between the measured signals is therefore allowed.

Looking at the time signal, a waveform can be observed at time t=0 as shown in Figure 5.20. Usually a trigger signal can be seen which looks rather like a pulse, but in this case a clear toneburst is visible.

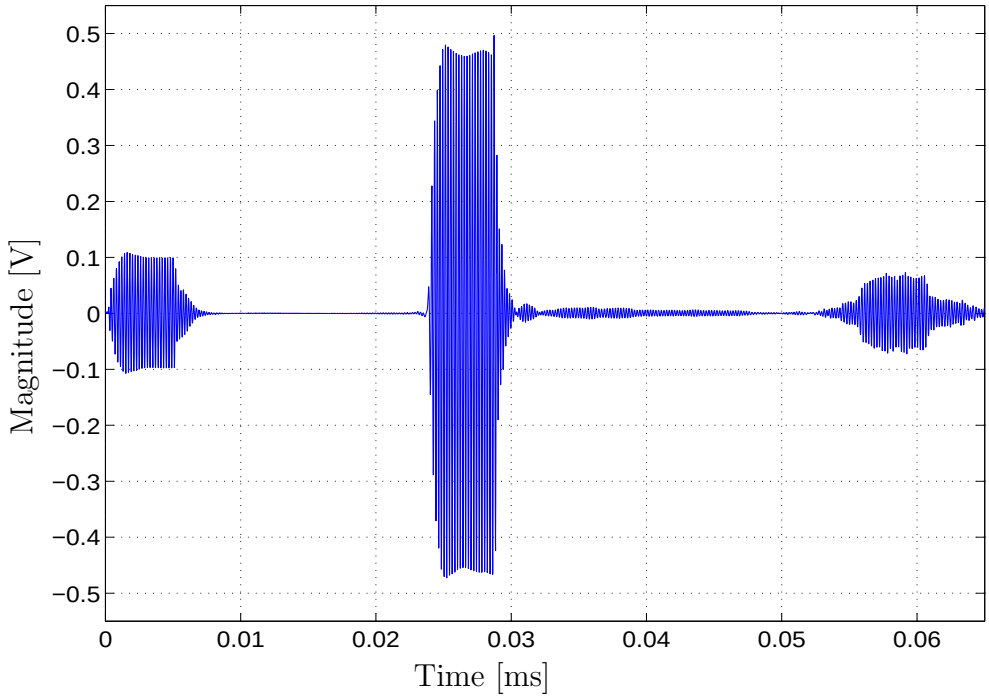

Figure 5.20: Time signal of a toneburst with 25 cycles, 5 MHz and a propagation distance of 4 cm

The explanation for this phenomenon is the bleed-through from the strong high power amplifier generating a toneburst at t=0 which is dominant in comparison to the regular trigger signal. This bleed-through does not affect the detected toneburst signal of the Rayleigh wave, therefore it can be neglected.

5.5.4 Nonlinear Ultrasonic Measurements and Problems Using the Conventional Setup #1

The experimental setup used in this set of measurements is explained in section 4.1, this setup is referred as the conventional experimental setup #1 in the following. The experimental procedure is basically the same as described above except that no fixture is used to change the propagation distance without changing the interface between wedge and specimen meaning that the wedge is moved relative to the specimen to enable measurements at different propagation distances.

A toneburst with 25 cycles and an input voltage of 800 mV is generated by a function generator, afterwards this sinusoidal signal is amplified with 50 dB and drives the ultrasonic transducer with 5 MHz.

Now different propagation distances are considered. Figure 5.21 shows a zoomed plot of the frequency domain for a propagation distance of 5.3 cm where peaks at 10 or 15 MHz can be seen.

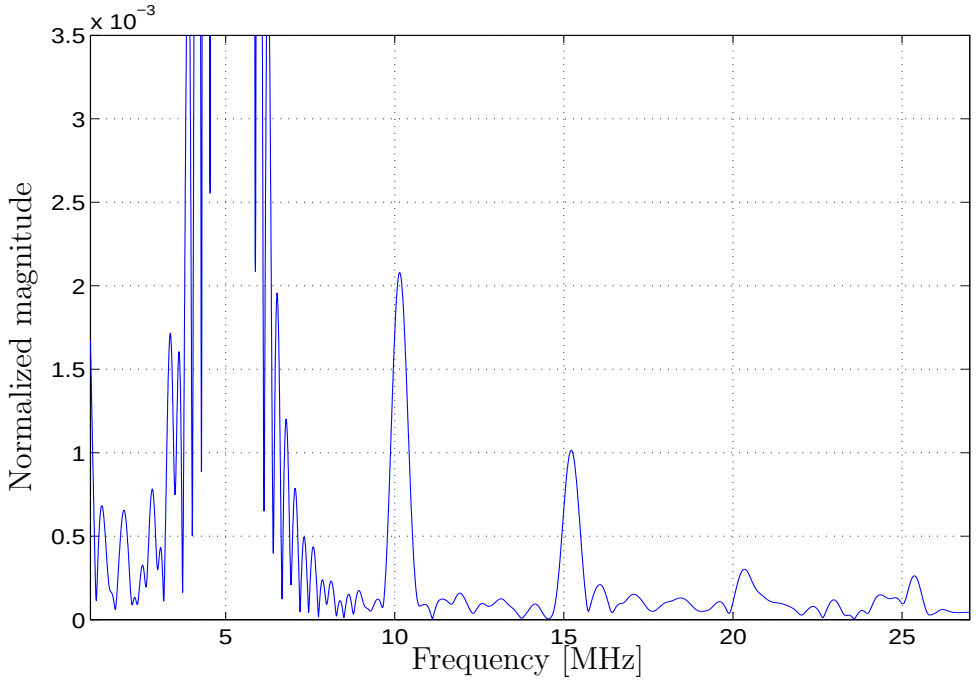

Figure 5.21: FFT of a toneburst signal with 25 cycles, 5 MHz and a propagation distance of 5.3 cm using setup #1

Figure 5.22 shows a signal for a propagation distance of 6.5 cm, Figure 5.23 provides a plot for a propagation distance of 3.7 cm. The alignment during the laser detection is almost the same for this set of measurements. The ratio between the normalized amplitude of the second order harmonic and the fundamental is around 2:1000.

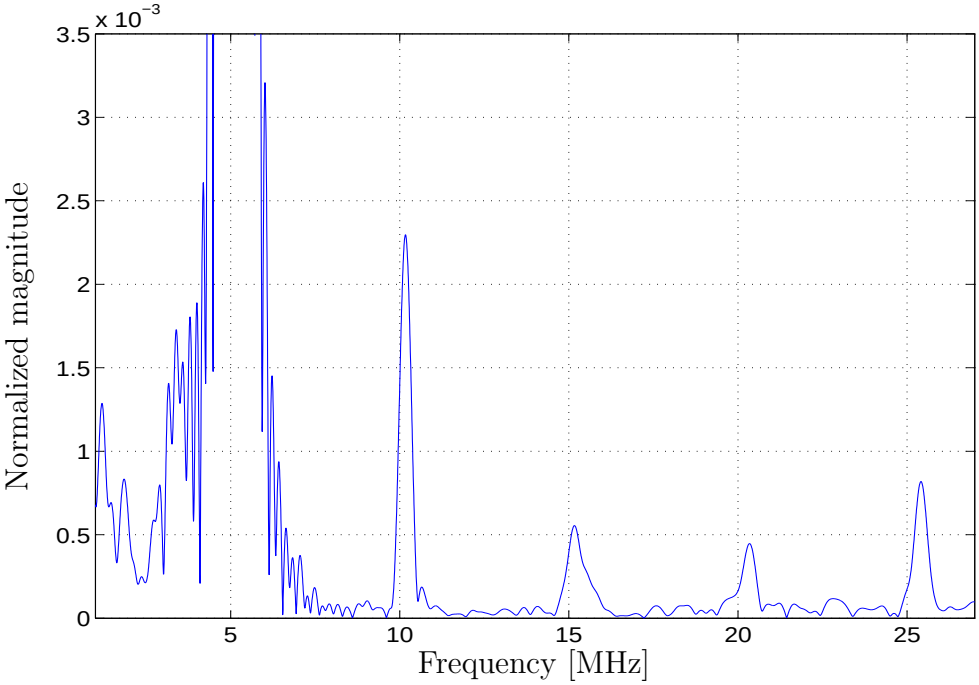

Figure 5.22: FFT of a toneburst signal with 25 cycles, 5 MHz and a propagation distance of 6.5 cm using setup #1

As mentioned earlier, the amplitude of the second harmonic has a linear relation to the propagation distance. Figure 5.24 shows the result of the measurements with three different propagation distances. It is clear that the second harmonic increases linearly with an increasing propagation distance which is the expected result. The longer the wave propagates, the more nonlinearity is added to the signal, therefore the second harmonic increases.

Theoretically the Rayleigh wave is a plane wave without loosing energy in the direction of propagation as mentioned in Section 5.4. Comparing the time signals

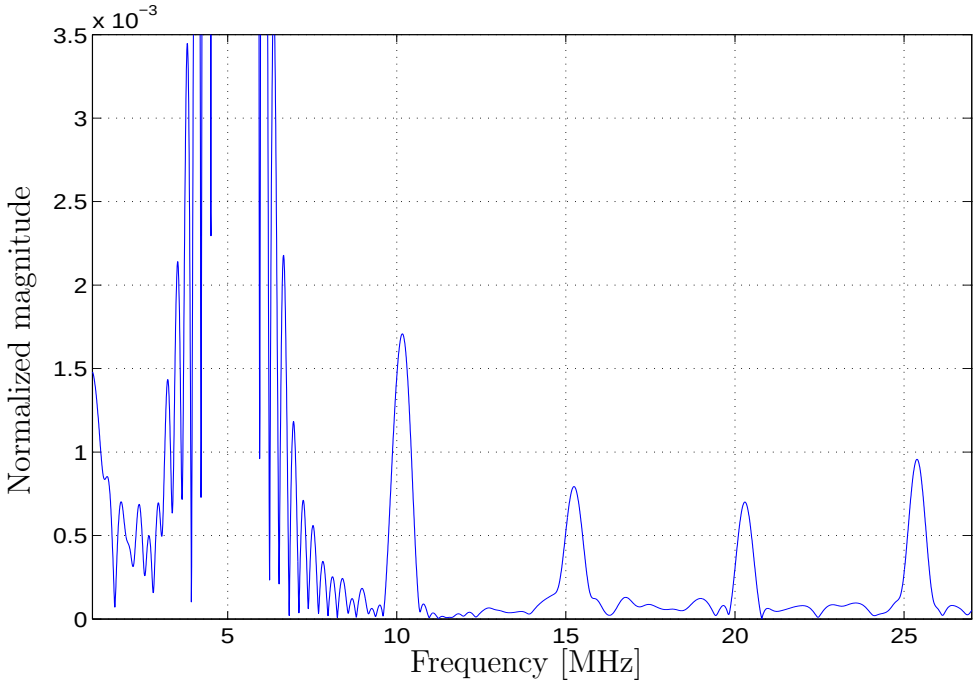

Figure 5.23: FFT of a toneburst signal with 25 cycles, 5 MHz and a propagation distance of 3.7 cm using setup #1

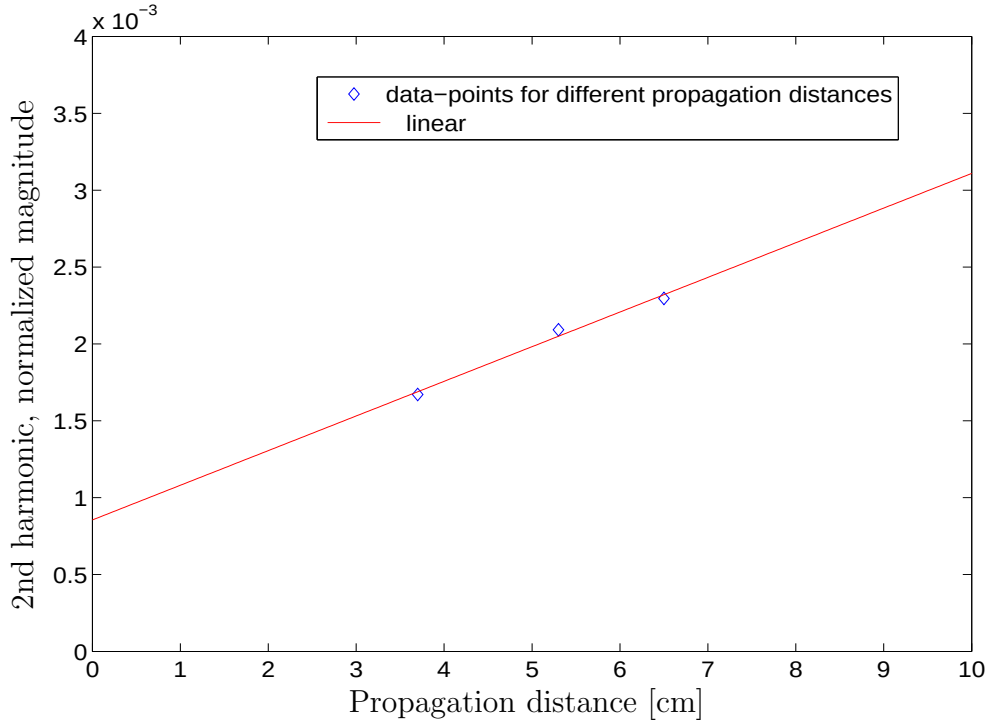

Figure 5.24: Normalized amplitude of the 2nd harmonic vs. propagation distance using setup #1

measured with setup #1, a variance of the peak-to-peak voltage from 0.18 V to 0.25 V is visible. For some reason, the output voltage of the detected signal propagating 6.5 cm (which is the largest propagation distance) is even higher than the one for the shortest propagation distance. A reasonable explanation is missing at this time. Probably geometrical effects affect the measured signal, especially if the propagation distance is very long.

Since the peaks in the frequency domain at 10 MHz are very small compared to the fundamental and large peaks at higher order harmonics can be seen as well, one has to be careful if the 10 MHz peak is really the amplitude of the second harmonic. Especially nonlinearity of the instrumentation is also added to the signal. To obtain more information about instrumentation nonlinearity, the input signal is investigated in the frequency domain which can be found in Figure 5.25. 25 cycles and an input voltage of 800 mV are generated by the Wavetek function generator, then the signal is amplified using the same 50 dB amplifier used for the nonlinear measurements. The signal is shown at the oscilloscope right before it goes to the ultrasonic transducer, then the FFT algorithm is used to get the information in the frequency domain.
One can see that high peaks at frequencies of higher harmonics occur, the dominant peak is at 15 MHz. According to Maess [15], this behavior is typical for electrical devices like the 50 dB amplifier. Electrical equipment tends to generate odd order harmonics, but also a peak at 10 MHz can be seen. The question is now if the peaks at 10 MHz, investigated during the nonlinear ultrasonic measurements, are really amplitudes of the second harmonic or rather due to the instrumentation. Even though the piezoelectric transducer acts like a band-pass filter so that the instrumentation nonlinearity is filtered out partially, there is still a contribution from the instrumentation to the nonlinearity parameter. To sum up, one can say that the peak at 10 MHz (see Figures 5.21, 5.22, 5.23) consists of the second harmonic and the nonlinear

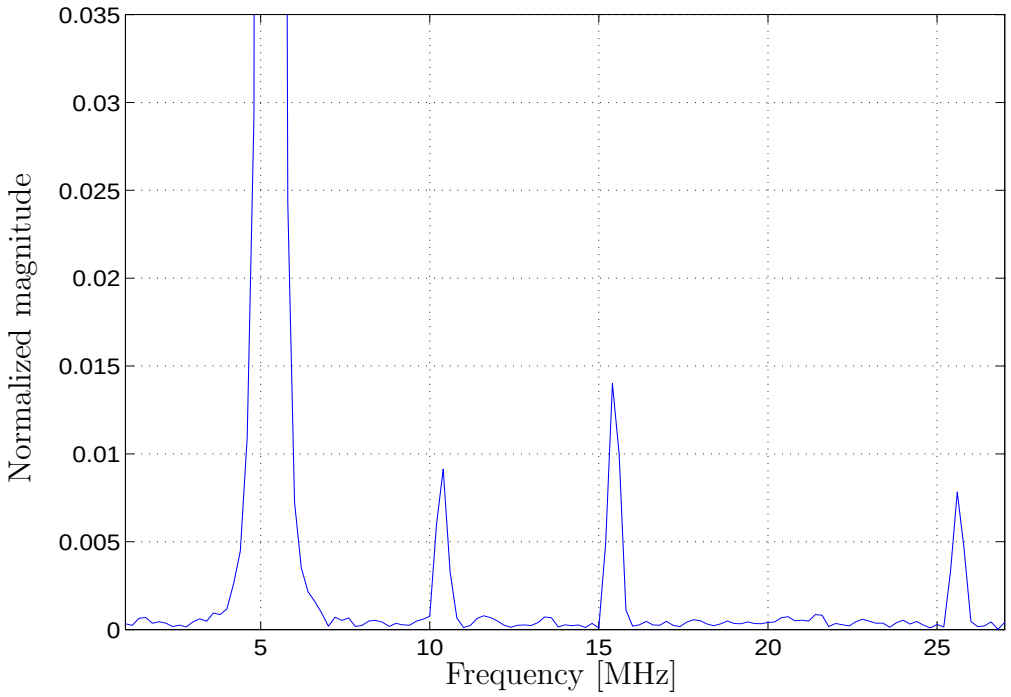

Figure 5.25: FFT of the input signal

portion of the equipment.

According to the literature, there is also a linear relationship between the third order harmonic and the propagation distance, but as you can see from the plots, this relationship is not observed. As mentioned above, the peak at 15 MHz is highly influenced by the instrumentation, in particular by the amplifier.

Besides the laser detection system behaves linearly up to 10 MHz, but because the 3rd order harmonic is at 15 MHz, nonlinearity could be already in the system due to the laser interferometer. Even with an amplifier designed for nonlinear measurements, it is therefore quite difficult to obtain consistent results for a linear dependence of the 3rd order harmonic on propagation distance, unless it is excited sufficiently above the instrumentation nonlinearity.

As in the preceding section, one can check the system linearity of the experimental setup — a linear relationship between the amplitude of the 2nd harmonic A_2' and the

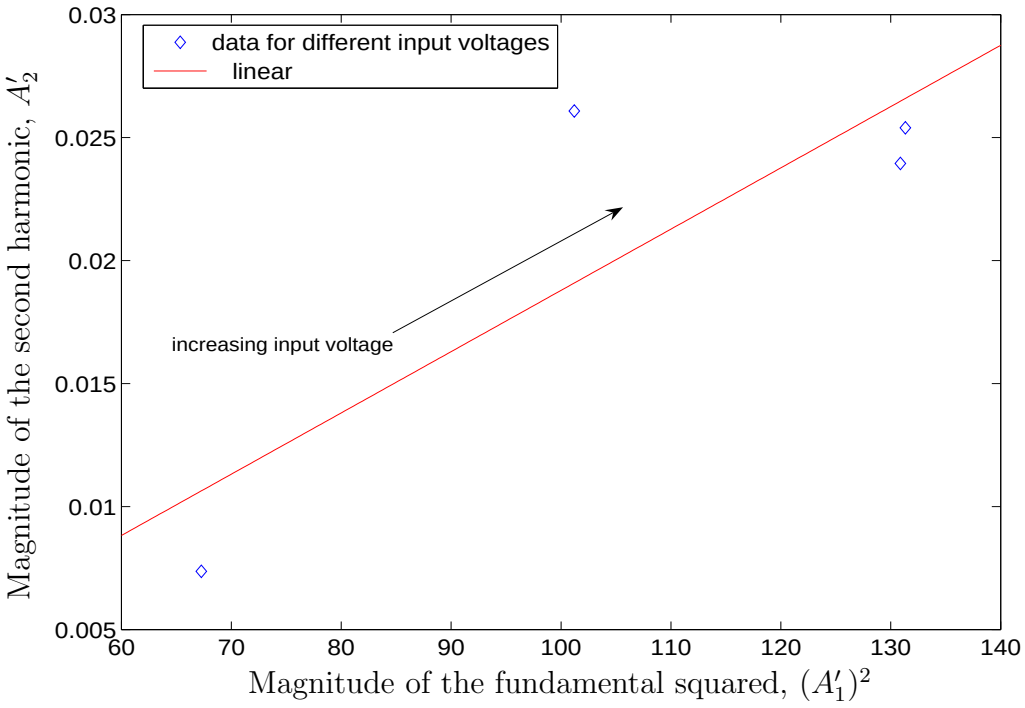

Figure 5.26: Amplitude of the second harmonic versus the squared amplitude of the fundamental wave for different input voltages

squared amplitude of the fundamental ${A_1'}^2$ for different input voltages. Figure 5.26 shows such a plot for setup #1 with an input voltage which varies from 400 mV to 900 mV (this is the voltage before amplification). The data is based on the measurement with a propagation distance of 5.3 cm. For instance, Figure 5.21 shows the signal with an input voltage of 800 mV. From Figure 5.26, it is clear that a linear relationship is not visible. Especially the amplifier tends to generate a high nonlinearity to the setup. Therefore an amplifier designed for nonlinear ultrasonic measurements (such as RAM-10000 used in setup #2) is needed because only then, the amplitude of the second harmonic can be detected in an accurate way without any disturbances due to the experimental setup. Another possibility to get better results would be a high voltage band-pass filter which can be used after the amplifier and right before the input signal goes in the transducer. The disadvantages of such a filter are that it is relatively expensive and it attenuates ($\approx$ 6dB) the high voltage signals.

Despite all the uncertainties mentioned above, the plot showing the linear increase of the amplitude of the second harmonic with propagation distance (Figure 5.24) is still conclusive because a system nonlinearity would affect the signal at 10 MHz in the same way for all the propagation distances. Even if not only the second harmonic is measured, a linear increase of the amplitude should still be visible. But the measurements are neither reliable nor repeatable because the system nonlinearity is dominant and especially if one wants to compare different specimens with different damage states, one has to come up with a better experimental setup for nonlinear ultrasonic measurements. It is obvious from Section 5.5 that the experimental setup #2 fulfills these requirements, therefore it is used in the following chapter to investigate and quantify material nonlinearity.

5.5.5 Transducer Nonlinearity

Especially the amplifier particularly designed for nonlinear acoustic measurements (RAM-10000) leads to improvements concerning system linearity and efficiency. It is also interesting to see how a different transducer affects the experimental results. A second PZT-transducer (transducer #2) is attached on the wedge the same way as before and a nonlinear ultrasonic measurement is performed for a Rayleigh wave propagation distance of 3.8 cm; Specimen 2a is used for this measurement. Figure 5.27 compares the two different transducers in showing the Fourier spectrum. A large peak at 10 MHz is visible for transducer #2. This means that this particular transducer induces a high nonlinearity, therefore the peak at 10 MHz is not the real second harmonic from the material one is looking for, but rather the nonlinear transducer behavior. It is obvious that transducer #1 (which has been used so far) is the better choice for nonlinear measurements. Throughout the measurements it has turned out that this particular commercial PZT-transducer is relatively linear.

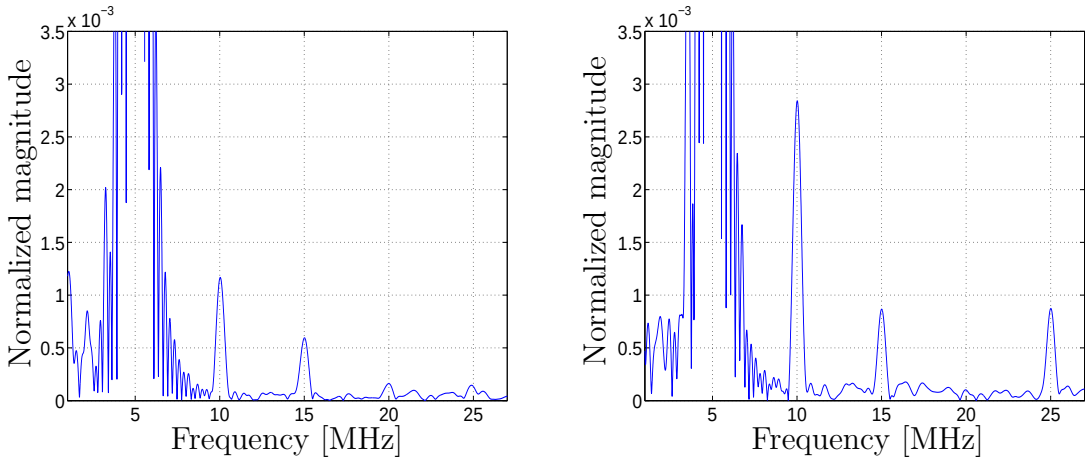

(a) Transducer #1 (b) Transducer #2

Figure 5.27: Comparison of two different PZT-transducers, Rayleigh wave propagation distance of 3.8 cm

CHAPTER VI

EXPERIMENTAL RESULTS - QUANTIFICATION OF MATERIAL NONLINEARITY

Different surface conditions and damage states with respect to higher harmonics and nonlinear wave propagation are compared in this chapter. It has been shown in chapter 5 that the experimental setup #2 is effective for nonlinear acoustic measurements, therefore it is used for the experiments described in this Chapter.

6.1 Surface Effects

Because Rayleigh waves travel along the surface of the specimen and because of the sensitivity of nonlinear ultrasonic measurements, it is important to know how a certain surface condition affects the detection of higher harmonics.

So far only a machined specimen has been used to detect nonlinearity in the material. A clear linear increase of the second harmonic with propagation distance could be seen. Now a second specimen (Specimen 2, see Table 4.2) of the same material (nickel base superalloy) is used to investigate surface conditions: First, the specimen is polished, sanded and lapped and nonlinear ultrasonic measurements are performed. Surprisingly the normalized amplitude of the second harmonic stays almost constant for different propagation distances, although one can see a trend that the second harmonic increases linearly with propagation distance at a lower level (Figure 6.1). A reasonable explanation could be that the sanding and lapping of the surface removed the nonlinear effects measured with the other specimens so far.

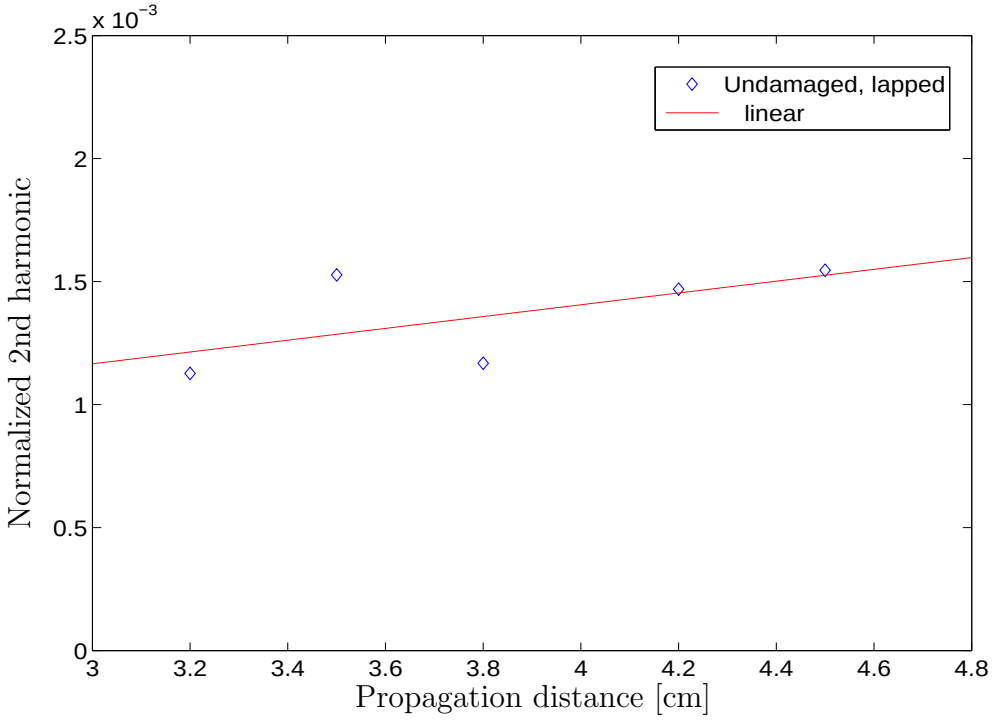

Figure 6.1: Second harmonic over propagation distance for a lapped and sanded specimen

Another interesting surface condition is an oxide layer on the surface of the specimen. In technical applications nickel base superalloys are common materials in the high temperature regime, therefore the surface is usually oxidized. It is important to see if this oxide layer has influence on the nonlinear effects and in particular the second harmonic.

To create an oxidized surface, one can simply put the sanded, polished and unoxidized specimen in a large keith furnace and heat it up with $10°C/min$ to $634°C$ and hold it for 600 min. Afterwards an oxide layer is clearly visible and the nonlinear ultrasonic measurement is repeated for a propagation distance of 4.5 cm because at this particular propagation distance the surface is relatively reflective and shiny and the laser detection is feasible. The result for the normalized amplitude of the second harmonic is compared to the unoxidized specimen in Figure 6.2.

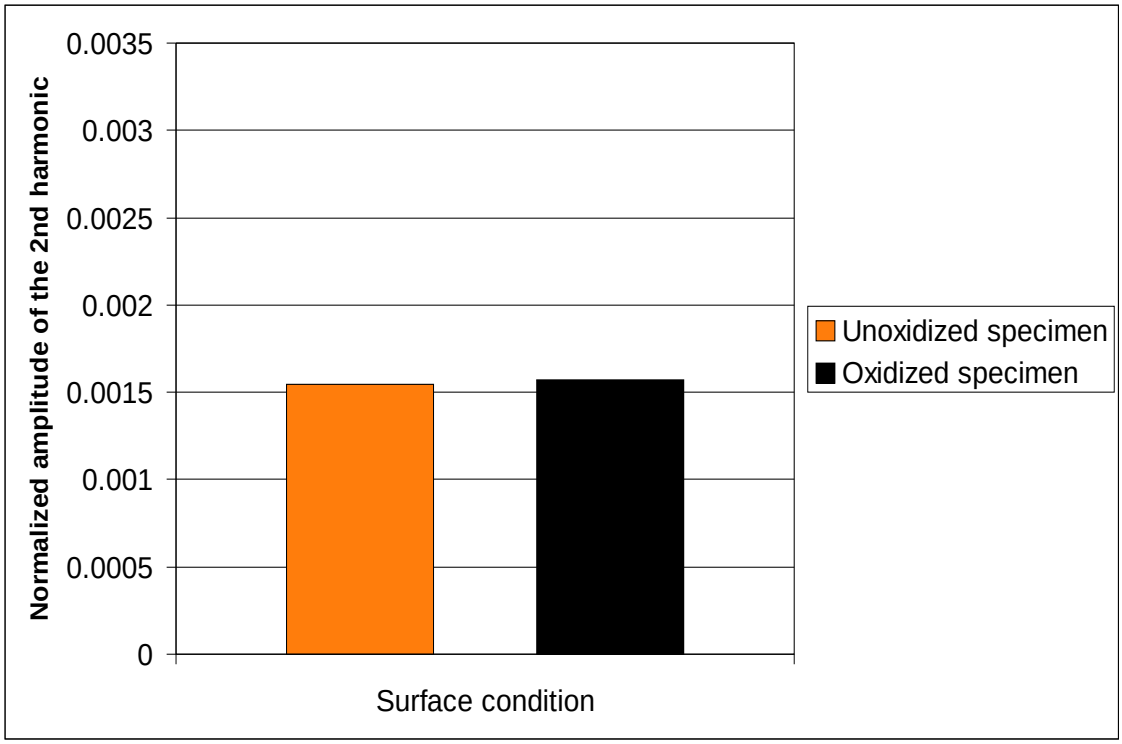

Figure 6.2: Second harmonic for different surface conditions

It is obvious that there is basically no difference in the amplitude of the second harmonic, therefore one can conclude that an oxide layer does not affect the nonlinear ultrasonic measurements. Moreover this conclusion is useful for investigating and analyzing fatigue tests: High temperature fatigue tests result in oxidized and damaged surface conditions and so far it was not clear if an oxide layer generates higher harmonics or if the contribution due to oxidization can be neglected.

Dirty and oxidized surfaces are very common in technical applications. Because such an oxide layer does not seem to contribute to the material nonlinearities, a comparison between specimens with different surface conditions is allowed. Nonlinear ultrasonic measurements appear to be a robust technique to detect higher harmonics and therefore accumulated fatigue damage in field applications and not only in the laboratory.

6.2 Damage Assessment by Nonlinear Ultrasonic Measurements

So far, only undamaged samples and the dependence of higher harmonics on propagation distance have been investigated. As mentioned earlier in Chapter 3, dislocations contribute to material nonlinearity and changes in microstructure. To examine the influence of dislocations on the generation of higher harmonics, this section deals with damaged and fatigued samples. Typically, fatigue damage is initiated at the surface, therefore a propagating Rayleigh wave is expected to generate higher harmonics (second order in particular).

In metallic alloys dislocation contribution to the material nonlinearity is considerably larger than the contribution due to lattice anharmonicity [8]. Especially cyclic loading promotes the formation of dislocation dipoles which results in increased levels of harmonic energy generation.

Section 6.2.1 and 6.2.2 investigate the influence of damage on higher harmonic generation whereas Section 6.2.3 and 6.2.4 present the results of a high-cycle and a low-cycle fatigue test.

6.2.1 Combined Loading - Monotonic Above Yield, Followed by Fatigue

To see if the developed experimental technique is able to detect damage, an undamaged, polished and lapped specimen is compared with a highly damaged one with respect to the generation of the second harmonic.

A MTS (Material Testing System) testing-machine with a force capacity of 100 kN is used to apply a load on the Specimen 2a leading to a stress level above yield (130% yield stress), and then 1000 cycles close to yield are applied. Figure 6.3 summarizes the results that compare the undamaged and damaged state showing that there is a significant increase in the second harmonic. It is obvious that the second harmonic increases with damage. Surprisingly, the magnitude stays almost constant

for the different propagation distances. An explanation could be that the damage is very localized and its affect is averaged out with increasing propagation distance. It is important to note the overall increase in the normalized second harmonic from undamaged to damaged states.

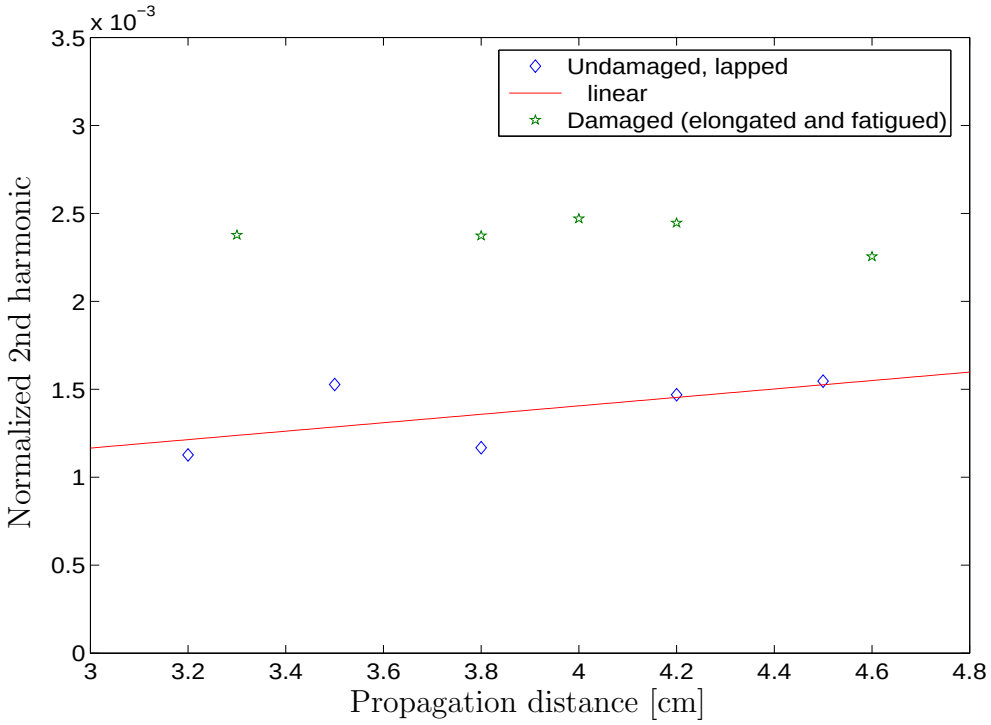

Figure 6.3: Second harmonic for different damage states

6.2.2 Monotonic Loading

To investigate damage accumulation and the dependence of the nonlinearity parameter β' on plastic deformation, a new set of specimens are used (Specimen 3). The geometry is similar to Specimens 1 and 2, except that this specimen consists only of the gage section, it is essentially a rectangular bar with the same sample thickness and width than used before. The geometry of Specimen 3 can be found in Figure 4.12. Because the second harmonic and the harmonic ratio (or β') increases with plastic deformation, a monotonic loading above yield is applied. The load is increased with 200 lbf/sec to an absolute end level which is equivalent to 115 % of the yield stress. Then

the specimen is unloaded with the same rate and nonlinear ultrasonic measurements are performed the same way as described earlier. The Rayleigh wave propagation distance is kept constant as 3.2 cm. The same procedure is repeated for a load equivalent to 125 %, 135 % and 145 % of yield stress (145 % of yield stress is close to the ultimate strength of the material), the results can be found in Figure 6.4. Moreover

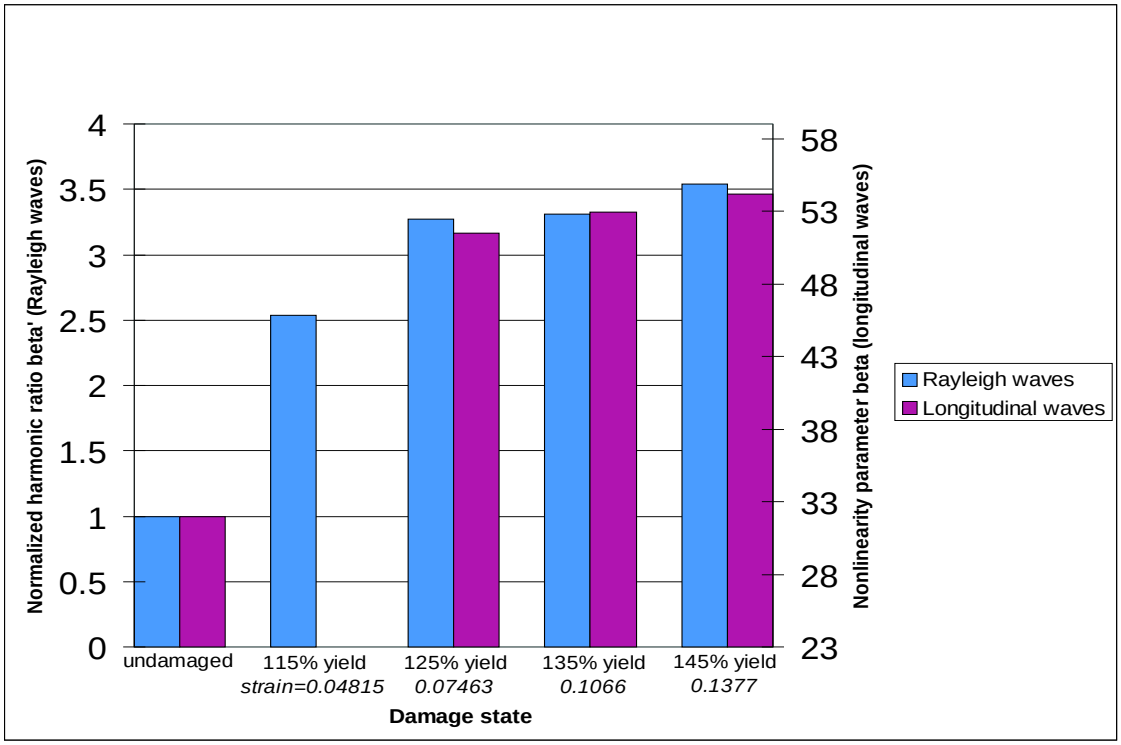

Figure 6.4: Normalized harmonic ratio β' vs. damage state, Rayleigh wave propagation distance of 3.2 cm + comparison with bulk-wave measurements

the results for Rayleigh waves are compared with nonlinear bulk-wave (longitudinal wave) measurements for the same specimen [9]. These bulk-wave measurements are absolute and through the thickness of the material.

A large increase in β' with increasing stress and strain is visible. The trend is the same for longitudinal waves and the nonlinearity parameter β, although the harmonic ratio using Rayleigh waves seem to be more sensitive to plastic deformation.

The levels of β' (and β) after 125 % yield could be explained by the macroscopic damage on the surface of the specimen.

6.2.3 High-Cycle Fatigue Test

In the literature several definitions of high-cycle and low-cycle fatigue tests can be found. Usually one refers to a high-cycle fatigue test (HCF) when the cyclic stress is below yield, meaning that many cycles have to be applied to damage the material whereas a low-cycle fatigue test (LCF) induces plastic deformation even in the beginning of the fatigue test.

For the present HCF test, the cyclic stress is held constant at 96 % of yield stress and the frequency of cyclic loading is 1 Hz. Nonlinear ultrasonic measurements are performed at different damage or fatigue states. A plot for β' over fatigue life is shown in Figure 6.5. 100 % of fatigue life means that the specimen failed (200000 cycles for the present HCF test).

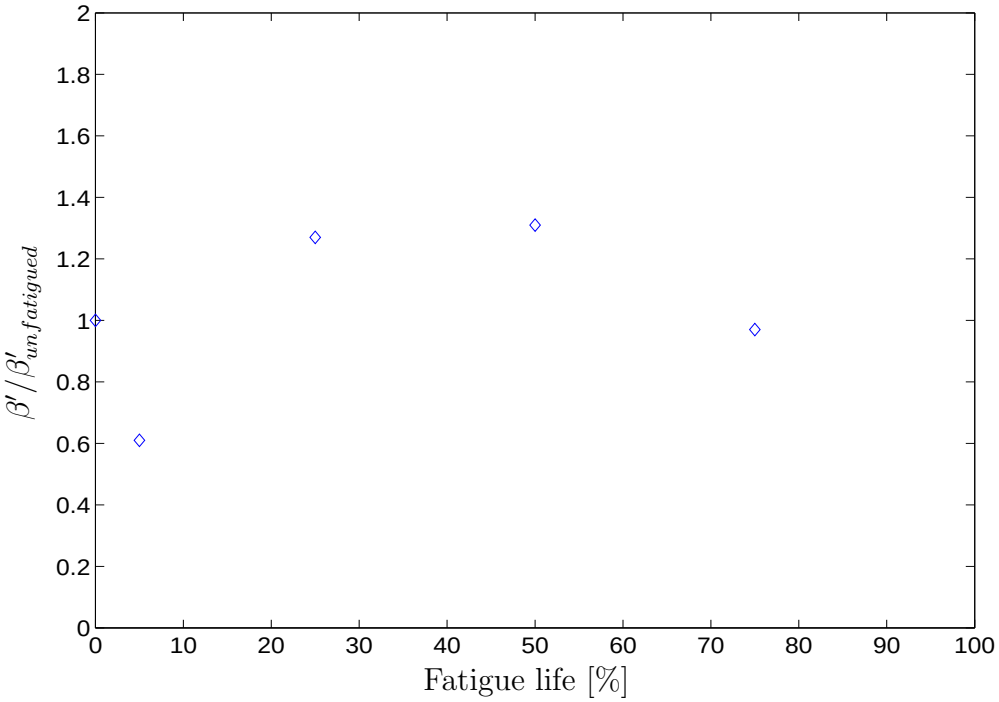

Figure 6.5: Normalized harmonic ratio β' over fatigue life for a high-cycle fatigue test and a Rayleigh wave propagation distance of 3.2 cm

There are no obvious conclusions available in this plot. Surprisingly, the value for β'

drops in the beginning, then it increases as expected for a fatigue life of 25 and 50 % but the value drops again for a fatigue life of 75 %. An explanation for this last drop in β' could be a microscopic surface crack with a crack tip larger than the wavelength of the second harmonic wave meaning that such a crack could cancel or delete the propagation of higher harmonics. The decrease of β' at the beginning of the HCF could be a result of the variability of the experimental setup — the transducer behavior possibly changed before the HCF was started. Moreover the interface between wedge and specimen changed after every fatigue step to refresh the couplant. It has been shown in section 5.5.2 that the measurements are still repeatable, but of course one has to take a certain variance into consideration.

6.2.4 Low-Cycle Fatigue Test

This section provides the results of a low-cycle fatigue (LCF) test. Strain-controlled loading is applied to ensure that the cyclic stress is above yield strength. The frequency of cyclic loading is 0.5 Hz. Figure 6.6 shows the normalized harmonic ratio, β', as a function of fatigue life. As mentioned earlier, 100% of fatigue life means that the specimen failed. This specimen (Specimen 5) failed after 12600 cycles. The Rayleigh wave propagation distance is 4.1 cm and for each measurement, three different input voltages are used and the measured values of β' are averaged.

From Figure 6.6 it is obvious that the value for β' increases with fatigue life, then the value drops for a fatigue life of 87 %. As mentioned in Section 6.2.3, this could be the result of a surface crack with a crack tip larger than the wavelength of the second harmonic. Barnard et al. [3] observed the same phenomenon for a low-cycle fatigue test.

For practical field applications, it is suggested that a linear and nonlinear surface wave

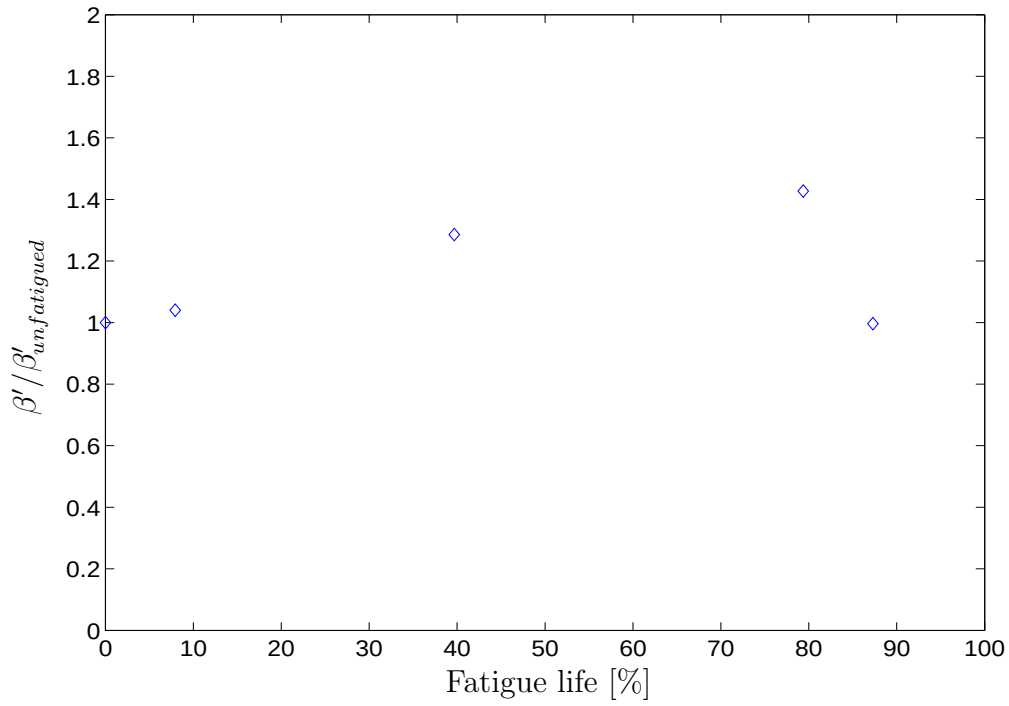

Figure 6.6: Normalized harmonic ratio β' over fatigue life for a low-cycle fatigue test

measurement is performed simultaneously so that the linear measurement monitors surface crack initiation while the nonlinear measurement evaluates material degradation.

CHAPTER VII

CONCLUSION AND POSSIBLE IMPROVEMENTS

This research demonstrates that contact wedge generation and non-contact interferometric detection are an efficient way to quantitatively measure higher harmonics in Rayleigh waves. The influence of the instrumentation on higher harmonics is investigated and an experimental setup is developed with a high system linearity to minimize spurious nonlinearities.

It is shown that in a nickel based superalloy, the second harmonic increases linearly with propagation distance. The level of the second harmonic changes for different surface conditions. A lapped and polished surface leads to a lower level of nonlinearity (the magnitude of the second harmonic) when compared to a machined surface, whereas an oxide layer shows no significant increase in nonlinearity.

Furthermore, the higher harmonics of Rayleigh waves are used to track micro-damage caused by applied load (the micro-damage is most likely associated with the accumulation of dislocations). It is shown that plastic deformation results in a significant increase in the second harmonic and the harmonic ratio β'. This harmonic ratio β' of Rayleigh waves seems to be more sensitive to plastic deformation than the nonlinearity parameter β for longitudinal waves.

A fatigue test with loading below yield (as realized in a high-cycle fatigue test) shows no conclusive results whereas a low-cycle fatigue test shows a consistent increase in the harmonic ratio, β', as a function of fatigue life until β' drops before the failure of

the specimen.

Throughout this research, the efficiency and the system linearity of the generation side are seen as the keys to obtaining reliable experimental results with respect to nonlinear wave propagation in Rayleigh waves.
A high input voltage is needed to generate the higher harmonics; these higher harmonics are small compared to the amplitude of the fundamental frequency. The gated high power amplifier used for experimental setup #2 fulfills the requirement of producing high voltage with a high system linearity for input voltage and trigger. This high voltage goes directly to the transmitting transducer which is not designed for nonlinear acoustic measurements meaning that the transducer itself has already a certain nonlinearity. A possible improvement would be a $LiNbO_3$ single-plate transducer which is seen as a highly linear transmitting transducer. Admittedly, it is not easy to attach this single-plate transducer on the plastic wedge with appropriate couplant and electrodes, that's the reason why it was not realized in this research but it is clear that $LiNbO_3$-crystals (as described in [4] and [28]) have great potential in nonlinear acoustic measurements.
Additionally, a high voltage filter could be used right after the amplification to ensure that the transducer is only driven with the fundamental frequency and not with the frequencies of higher order harmonics due to instrumentation.

Oil as couplant between the wedge and specimen (together with a fixture to hold the wedge firmly against the specimen) led to an improvement in efficiency compared to cement glue as couplant. The same improvement is expected for the interface between transducer and wedge, but because of the sloping surface of the wedge and shortage of space, it is hard to design a fixture to hold the transducer, that's why fluid coupling haven't been realized so far. To overcome this shortcoming, a thread could be applied

to the transducer or a small device could be designed which is attached on the sides of the wedge with the capability of pressing the transducer on the wedge.

A FFT-algorithm is used as a way to separate the higher harmonics in Rayleigh waves from the fundamental frequency in the frequency domain. So far, only the transformed magnitudes are compared and analyzed. To obtain the true values of higher harmonics, one has to transform backwards or use a pulse inversion technique where the second harmonic can be fully extracted from the fundamental by superposing two waveforms with a phase-shift of 180° (details can be found in the Appendix). Once having true values of higher harmonics, one can calculate a similar dimensionless nonlinearity parameter than the one for longitudinal waves for further comparisons between Rayleigh and bulk waves with respect to nonlinear wave propagation.
To obtain confidence intervals and error bars, nonlinear acoustic measurements have to be repeated for several samples. In this research, confidence intervals and statistical analysis are missing.

APPENDIX A

PULSE INVERSION TECHNIQUE

The second harmonic signal is small and very hard to extract from the fundamental. So far, the fast Fourier technique has been applied to separate the fundamental wave from higher harmonics in the frequency domain. Because of the large Rayleigh wave propagation distance throughout this research one could use a toneburst with many cycles to obtain a big and dominant steady-state portion of the signal. But if the propagation distance is small and only a short waveform can propagate, one has to come up with a more appropriate technique to extract the second harmonic component. Another disadvantage of the FFT is the fact that one only obtains transformed magnitudes in the frequency domain and not the real values.

The pulse inversion method is a way to solve the problems mentioned above. Ohara et al. [19] describe higher harmonic measurement by pulse inversion for the evaluation of amorphous diffusion bonding. The concept of pulse inversion consists of digital signal processing superposing two transmitted waves with a phase shift of 180°. The 180° difference of the fundamental is equal to a 360° difference of the second harmonic wave, hence the second harmonic can be extracted by superposing each transmitted waveform.

The two transmitted waveforms can be written as

$$u_1 = A_1 sin(\omega t - kx) + A_2 sin2(\omega t - kx) \tag{A.1}$$

$$u_2 = A_1 sin(\omega t - kx + \pi) + A_2 sin2(\omega t - kx + \pi). \tag{A.2}$$

Superposing equation A.1 and A.2 results in

$$u = u_1 + u_2 = 2A_2 sin2(\omega t - kx), \tag{A.3}$$

thus the second harmonic component with a doubled amplitude is obtained.

Figure A.1 shows the extracted 2nd harmonic signal for a Rayleigh wave propagation distance of 4.6 cm along a unfatigued specimen. Although the signal is small

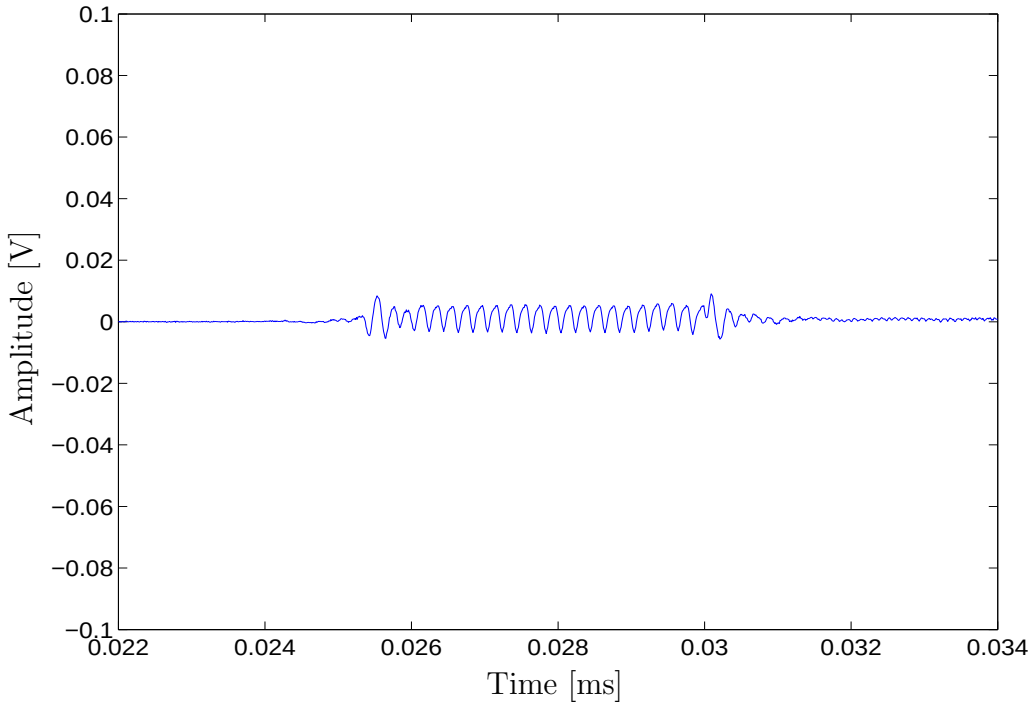

Figure A.1: Superposed waveform or extracted 2nd harmonic

compared to the fundamental, it is clearly visible and the pulse inversion technique is applied successfully. A comparison of the time signal with respect to the measured voltage shows that the absolute magnitude of the extracted signal is about 1 % of its fundamental.

Nevertheless the fundamental wave is still involved in the extracted signal because one can also see a 5 MHz-peak (fundamental frequency) in the frequency spectrum (see figure A.2) and not only the frequency of the 2nd harmonic. A rectangular window has been applied to the extracted time signal (note that the rectangular window was not sufficient before). To filter out the portion of the fundamental frequency, one

has to come up with a correlation technique to make sure that the two superposed signals start at exactly the same time.

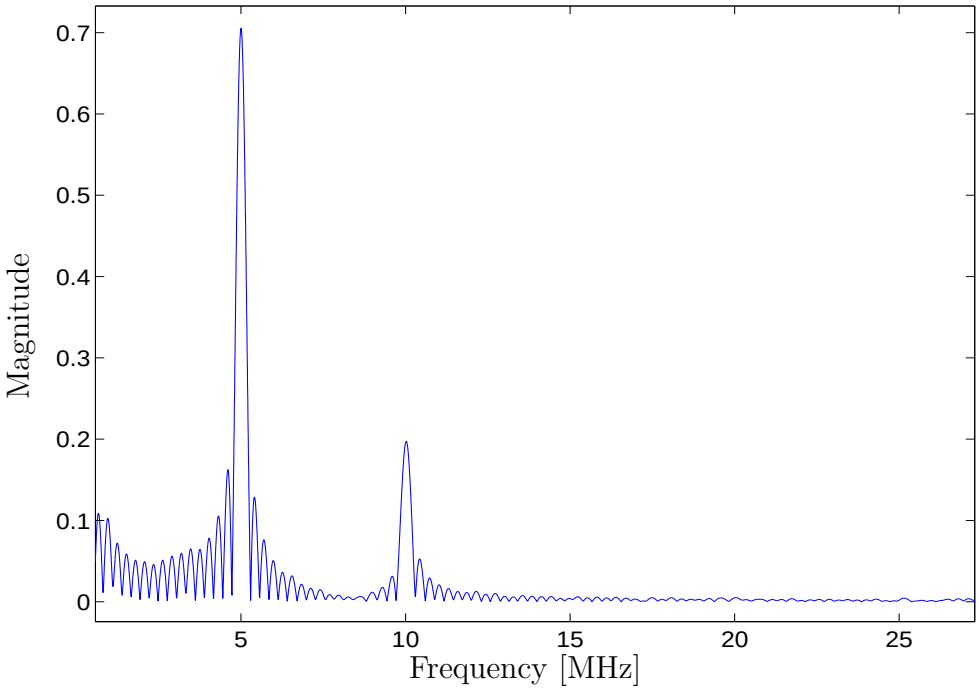

Figure A.2: FFT of the extracted time signal

REFERENCES

[1] Achenbach, J. D., *Wave Propagation in Elastic Solids*. Dover, first ed., 1975.

[2] Akira Hikata, B. B. C. and Elbaum, C., "Dislocation contribution to the second harmonic generation of ultrasonic waves," *Journal of Applied Physics*, vol. 36, no. 1, pp. 229–236, 1964.

[3] Barnard, D. J., Brasche, L. J. H., Raulerson, D., and Degtyar, A. D., "Monitoring fatigue damage accumulation with Rayleigh wave harmonic generation measurements," *Review of Quantitative Nondestructive Evaluation*, vol. 22, pp. 1393–1400, 2003.

[4] Barnard, D. J., Dace, G. E., and Buck, O., "Acoustic harmonic generation due to thermal embrittlement of Inconel 718," *Journal of Nondestructive Evaluation*, vol. 16, no. 3, pp. 67–75, 1997.

[5] Blackshire, J. L., Sathish, S., Na, J., and Frouin, J., "Nonlinear laser ultrasonic measurements of localized fatigue damage," *Review of Quantitative Nondestructive Evaluation*, vol. 22, pp. 1479–1488, 2003.

[6] Bruttomesso, *Laser Ultrasonic Techniques to Determine the Influence of Geometric Features on Rayleigh Waves*. Doctoral thesis, School of Civil and Environmental Engineering, Georgia Institute of Technology, 2002.

[7] Cantrell, J. H., "Substructural organization, dislocation plasticity and harmonic generation in cyclically stressed wavy slip metals," *Proc. R. Soc. Lond. A*, pp. 757–780, 2004.

[8] Cantrell, J. H. and Yost, W. T., "Nonlinear ultrasonic characterization of fatigue microstructures," *International Journal of Fatigue*, vol. 23, pp. 487–490, 2001.

[9] Davies, J., *Characterization of Microstructure Evolution of Nickel Based Superalloys Using Advanced Ultrasonic Techniques*. Master thesis, School of Mechanical Engineering, Georgia Institute of Technology, 2005.

[10] Deng, M., Wang, P., and Lv, X., "Experimental observation of cumulative second-harmonic generation of Lamb-wave propagation in an elastic plate," *Journal of Physics D: Applied Physics*, vol. 38, pp. 344–353, 2005.

[11] Ginzel, E. A. and Ginzel, R. K., "Ultrasonic properties of a new low attenuation dry couplant elastomer," *Ginzel Brothers & Associates Ltd.*, 1994.

[12] Hinton, Y. L., Na, J. K., Yost, W. T., and Kessel, G. L., "Field measurement of the acoustic nonlinearity parameter in turbine blades," *NASA Center for AeroSpace Information*, 2000.

[13] Hurlebaus, S., *Laser Generation and Detection Techniques for Developing Transfer Functions to Characterize the Effect of Geometry on Elastic Wave Propagation*. Master thesis, School of Civil and Environmental Engineering, Georgia Institute of Technology, 1996.

[14] Lardner, R. W., "Nonlinear Rayleigh waves: Harmonic generation, parametric amplification, and thermoviscous damping," *J. Appl. Phys.*, vol. 55, pp. 3251–3260, 1984.

[15] Maess, M., *Material Characterization Using Nonlinear Wave Propagation*. Master thesis, School of Civil and Environmental Engineering, Georgia Institute of Technology, 2001.

[16] Meyendorf, N. G. H., Nagy, P. B., and Rokhlin, S. I., *Nondestructive Materials Characterization*. Springer, first ed., 2003.

[17] Mueller, T., *Nonlinear Ultrasonics: Signal Processing Considerations and a Nonlinear Parameter for Rayleigh Waves*. Master thesis, School of Civil and Environmental Engineering, Georgia Institute of Technology, 2005.

[18] Nagy, P. B., "Fatigue damage assessment by nonlinear ultrasonic materials characterization," *Ultrasonics*, vol. 36, pp. 375–381, 1998.

[19] Ohara, Y., Kawashima, K., Yamada, R., and Horio, H., "Evaluation of amorphous diffusion bonding by nonlinear ultrasonic method," *Review of Quantitative Nondestructive Evaluation*, vol. 23, pp. 944–951, 2004.

[20] Oppenheim, A. V. and Schafer, R. W., *Discrete-time signal processing*. Prentice Hall, 1999.

[21] Planat, M., "Multiple scale analysis of the nonlinear surface acoustic wave propagation in anisotropic crystals," *J. Appl. Phys.*, vol. 57, pp. 4911–4915, 1985.

[22] Rose, J. L., *Ultrasonic Waves in Solid Media*. Cambridge University Press, first ed., 1999.

[23] Ruiz, A. and Nagy, P., "Diffraction correction for precision surface acoustic wave velocity measurements," *J. Acoust. Soc. Am.*, vol. 112, no. 3, pp. 835–842, 2002.

[24] Sachse, W. and Pao, Y.-H., "On the determination of phase and group velocities of dispersive waves in solids," *Journal of Applied Physics*, vol. 49, pp. 4320–4327, 1978.

[25] Scruby, C. B. and Drain, L. E., *Laser Ultrasonics, Techniques and Applications*. Adam Hilger, 1990.

[26] Shull, D. J., Hamilton, M. F., Il'insky, Y. A., and Zabolotskaya, E. A., "Harmonic generation in plane and cylindrical nonlinear rayleigh waves," *J. Acoust. Soc. Am.*, vol. 94, pp. 418–427, 1993.

[27] Viktorov, I. A., *Rayleigh and Lamb Waves, Physical Theory and Applications*. Plenum Press New York, first ed., 1967.

[28] Yost, W. T. and Cantrell, J. H., "Calibration techniques for electronic-based systems used in measurements of nonlinearity parameters," *Review of Quantitative Nondestructive Evaluation*, vol. 18, pp. 2345–2351, 1999.